I：地下水定年

I.1：Poster－Verification of He-4 and Cl-36 dating for very old groundwater in Great Artesian Basin, Australia

Verification of ^{4}He and ^{36}Cl dating for very old groundwater in Great Artesian Basin, Australia

[1]Takuma HASEGAWA, [2]Yasunori MAHARA, [1]Kotaro NAKATA, [3]M.A.Harbermehl

[1] Central Research Institute of Electric Power Industry. 1646 Abiko, Abiko-shi, Chiba-ken, Japan. e-mail: t-hase@criepi.denken.or.jp, k-nakata@criepi.denken.or.jp
[2] Kyoto University. Kumatori-cho, Sennan-gun, Osaka, Japan. e-mail: mahara@HL.rri.kyoto-u.ac.jp
[3] Bureau of Rural Sciences. Canberra A.C.T. 2601, Australia. e-mail: Rien.Habermehl@brs.gov.au

1. Background

The groundwater dating are one of the most promising methods to evaluate very slow groundwater flow. The residence time of groundwater is important for radioactive waste disposal. On radioactive waste disposal time range over ten-thousands or more is important. As shown in Figure 1, there are many dating methods. However, the applications of dating methods longer than ten-thousands or more are very limited, and the researches are still required. From this point of veiw, ^{36}Cl and ^{4}He dating will be useful tool. Therefore, it is imporant to conduct and validate these methods to in-situ investigation. In this study, ^{36}Cl and ^{4}He dating were conducted in the Great Artesian Basin. This study entitled 'Research and development on groundwater dating technique' was done under contracts awarded from METI (Ministry of Economy, Trade and Industry).

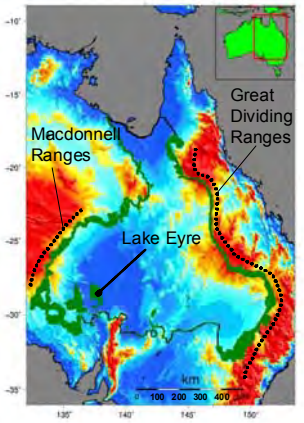

Location of Great Artesian Basin
(■ indicates outcrop of aquifer)

2. Principle of ^{36}Cl and ^{4}He dating

^{36}Cl dating

^{36}Cl is radioisotope of Chloride with a half-life of 3.01×10^6 y.

$$t = -\frac{1}{\lambda}\ln\left(\frac{R - R_{se}}{R_0 - R_{se}}\right)$$

Where t is the age, λ is the decay constant of ^{36}Cl, R is measured ^{36}Cl/Cl ratio, R_0 is the initial ^{36}Cl/Cl ratio, R_{se} is the seular equibrium

^{4}He dating

Helium is the noble gas. ^{4}He accumulates with time by in-situ production and external flux.

$$t = \frac{D - D_{eq}}{M + F/nb}$$

Where D is measured helium concentration, D_{eq} is atmospheric equilibrium, M is production rate from rock, n is porosity and b is aquifer thickness, F is external flux that depends on site. M is given by following equation.

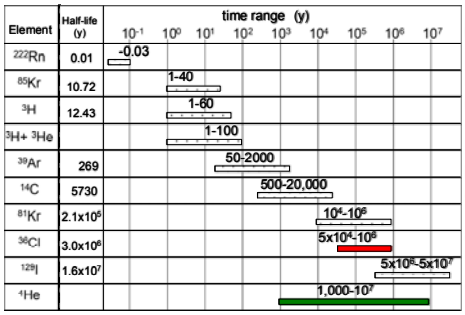

Dating methods and available time range

3. Study site

The Great Artesian Basin is one of the largest basin in the world. It occupies about one-fifth of Australia. The basin has a relatively simple bowlike structure and multi-layer system. The multi-layer system consit of quarzose and sandstone intervening confining layer of siltston, mudstone and shale. These layers outcrop at the edge of basin and tilte to south-west.

The advantage of Great Artesian Basin for very old groundwater daing are as follows, 1)Relatively simple groundwater flow because of simple geological structure, 2) Groundawter inflow and mixing are restricted because of arid or semi-arid and artesian condition, 3) Residence time will be longer than millions year because of very long flow line, 4) No large tectonic influence during millions year, 5) There are many boreholes and previous study because borewater is main water resource

4. Water sampling and analysis

From 2002 to 2003, 77 water sampling were collected from Cadona-owie Hooray aquifer, which is the top of artesian aquifer and mainly exposited. Temperature, pH, electric conductivity, Eh and dissolved oxygen were measured in-situ. Major ions, stable isotopes of d^{13}C, dD and d^{18}O, radioactive isotopes of ^{3}H, ^{14}C and ^{36}Cl, noble gases of^{4}He, ^{3}He/^{4}He and Ne were measured using sampling water.

5. Result and discussion

Measured major ions were expressed by stiff diagram at borehole location. There is a trend that dissolved solute increase along flow path. The distribution of ^{36}Cl/Cl and ^{4}He was drawn by kriging. The ^{36}Cl/Cl decreases with distance from recharge area due to radioactive decay. Especially, this trend is clear within hundreds kilo-meters from recharge area. The ^{4}He concentration increases with distance from recharge area due to ^{4}He accumulation. ^{4}He concentrations are quit low in the center of basin due to pressure lowering and boilling because the aquifer is over thousands meter from surface.

6. Summary

We applied ^{36}Cl and ^{4}He dating to Great Artesian Basin.

- ^{36}Cl age along the defined flow path are proportional to the distance of recharge area, therefore it was confirmed that ^{36}Cl age reflect residence time of groundwater.
-^{4}He concentration increases with distance near the recharge area. Moreover, there are close relationship with ^{36}Cl age. It shows that ^{4}He also reflect residence time.

From these results, it was confirmed that ^{36}Cl and ^{4}He dating are useful for very old groundwater.

However, for ^{4}He dating, ^{4}He accumulation rate is site specific and depends on the geological conditions. Careful investigations are required to estimate the external flux.

^{4}He concentration has large variation in the central basin because of degassing. Sampling method should be improved to eliminate degassing.

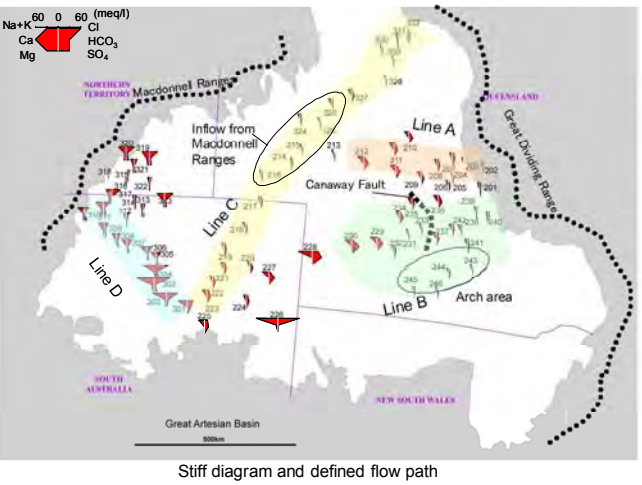

Stiff diagram and defined flow path

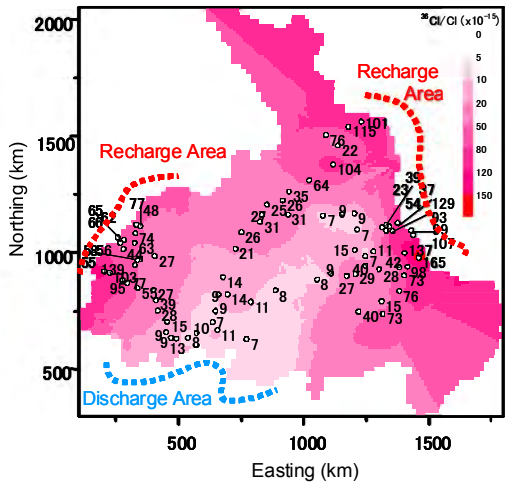

^{36}Cl/Cl distribution

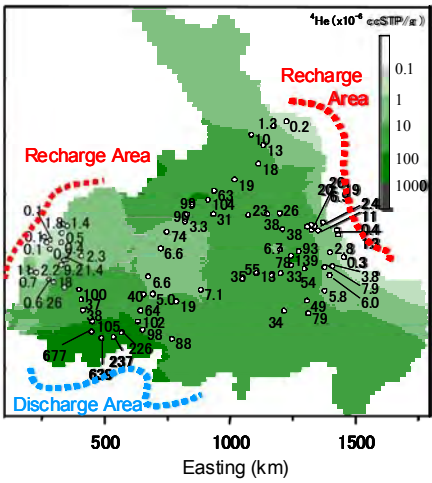

^{4}He distribution

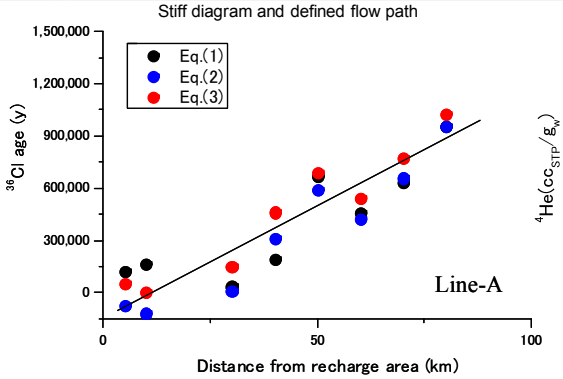

^{36}Cl age versus distance from recharge area

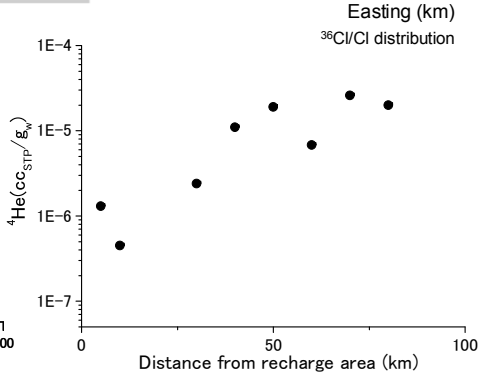

^{4}He concentration versus distance from recharge area

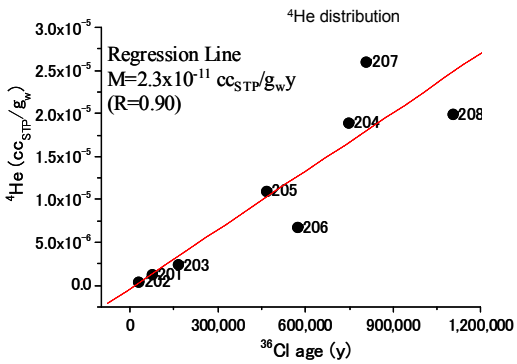

^{36}Cl age versus ^{4}He concentration

Acknowledgements

We thank to Prof. A.Kudo (Kyoto Univ.), Prof. T.Nakamura (Nagoya Univ.), Prof. J.Shimada(Kumamoto Univ.), Prof. M.Nishigaki (Okayma Univ.) and Assi. Prof.T.Tokunaga for kind addvice for this project. We also thank to Mr. Y.Mizuochi, Mr. H.Kobayashi and Mr. A.Ninomiya(SUMICON), Dr Ransley (BRS) for support of in-situ sampling and to Prof. F.Fifield (ANU) and Prof. M. Suter (ETH) for ^{36}Cl measurements.

I.2：Poster－Integration of groundwater flow simulation using groundwater chemistry and groundwater age

Integration of groundwater flow simulation using groundwater chemistry and groundwater age.

Takuma Hasegawa[1], Kotaro Nakata[1], Hirofumi Kondo[1],Keiichiro Goto[1], Shigenori Muramoto[2], Yuichi Tomioka[1], Kazuyuki Goto[1], Kouki Kashiwaya[3]

1. CRIEPI (Central Research Institute of Electric Power Industry), Abiko-shi, Japan.
2. NUMO (Nuclear Waste management Organization of Japan), Minato-ku, Japan.
3. Kumamoto University, Kumatomo-shi, Japan.

1. Introduction

On preliminary investigation of high level radioactive waste disposal, surface-based investigations (e.g. geological and borehole surveys) will be conducted. The numerical simulation of groundwater flow is one of the most promising methods to summarize the investigations. Moreover, numerical simulation is useful to identify key components for future investigations.

Cooperative research between NUMO and CRIEPI were conducted to borehole investigation up to 500 m in depth at west costal area in Miura Peninsular (Fig.1 and Fig.2). The conceptual model of groundwater flow was discussed using numerical simulations, which focus on total heads, salinity, ^{4}He concentration.

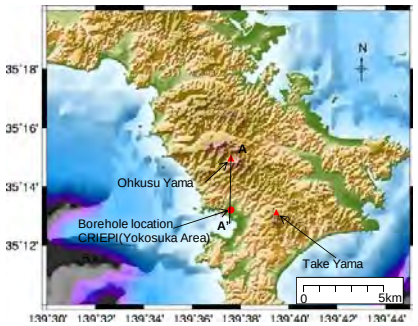

Fig.1 Land and seabed geography near borehole location (GSI(1997), Marine Safety Agency (2000), (2007).)

2. Borehole investigations

At borehole location, the Hayama G. distributed under 210 m in depth and the Miura G. overlaid the Hayama G. and distributed from ground level to 210 m in depth(Kondo et al., 2011).

As shown in Fig.3, Hydraulic conductivities of the Miura G. and the Hayama G. are approximately 1X10^{-7} m/s and 1X10^{-9} m/s, respectively.

Total head is almost constant and a few meters lower than the ground level in the Miura G. and increase with depth in the Hayama G. It is not clear to increase total head with depth whether density effect or discharge area.

Salinity is low upper 100 m in depth, and increase with depth and reach seawater level under 300 m in depth. It didnot depend on geological formation.

^{4}He concentrations are equivalent to atmospheric equilibrium upper 100 m in depth, and increases with depth and reaches appr. 2X10^{-5} cc_{STP}/g_W considering degassing under 300 m in depth, which is equivalent to 7 Ma accumulation in the Hayama G.

Moreover, ^{14}C was detected significantly in the Miura G (40-60 pMC), ^{36}Cl/Cl is equivalent to modern seawater level in the Miura G. and in situ equilibrium in Hayama G. From these results, groundwater is mobile in the Miura G. and stagnant in the Hayama G. Fossil seawater could be remained in Hayama G(Hasegawa et al. 2011).

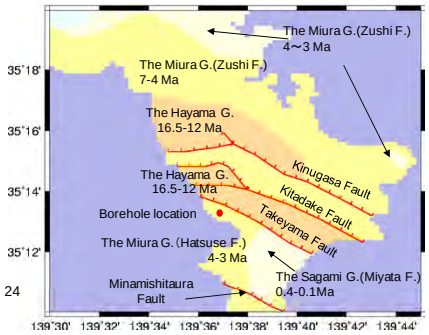

Fig.2 Geology and faults near borehole location revised Geological Survey of Japan(2003).

3. Simulation on groundwater flow and solute transport

Salinity and ^{4}He were simulated because 1) density of salinity influences to the groundwater and 2) salinity and ^{4}He provides important information of groundwater mobility. Modeling area was defined by considering local groundwater flow and maximum regression.

The governing equations of groundwater flow are mass balance and Darcy low considering density dependent flow.

Steady and unsteady state simulations were performed including sensitive analyses for hydraulic conductivity. Boundary conditions are shown in Fig.4. Unsteady state simulations considering sea level changes was assumed as follows, 1) periods of sea level change is 120 ka, transgression and regression are 20 ka and 100 ka, respectively. 2) maximum sea level changes is 140 m, which is maximum transgression +5 m and maximum regression -135 m from present sea level. 3) global uplift is considered as 50 m/100 ka Three cycle of sea level changes was simulated. Initial conditions are assumed as remained fossil seawater (7 Ma derived from ^{4}He dating) in both the Miura G. and the Hayama G.

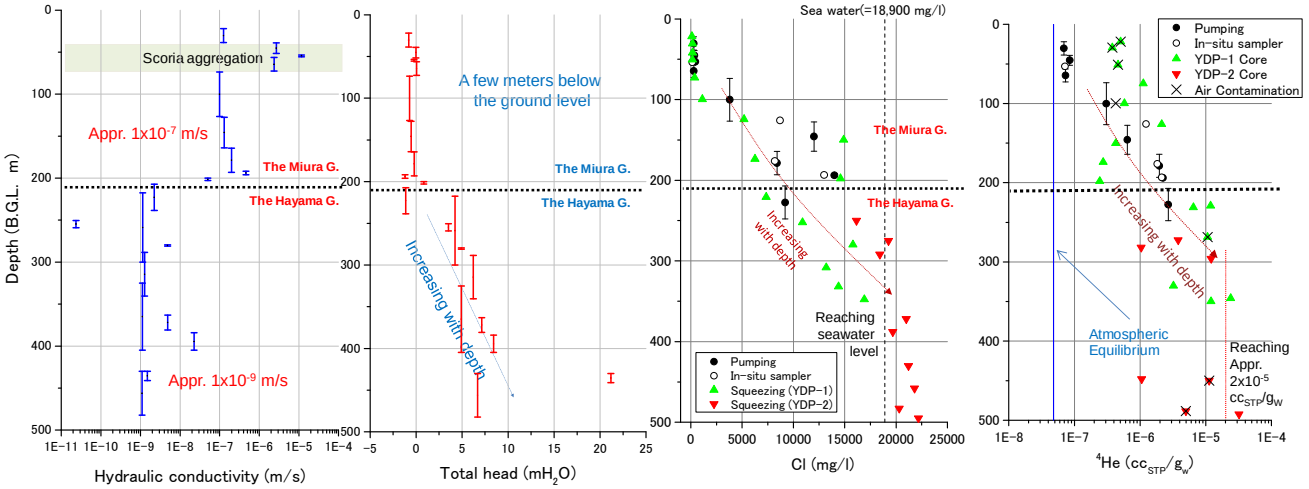

Fig.3 The results of borehole investigations

4. Simulation results

Steady state simulations could not reproduce total head and salinity(Fig.5). Total head could be reproduced neglecting fault as modeled by hydraulic barrier, however, simulated salinity and ^{4}He is very low compared to measured values. Especially salinity increasing from middle part of the Miura G. is difficult to reproduce by simulation.

Unsteady state simulation could reproduce the salinity as mentioned above(Fig.6). This salinity distribution in the Miura G. was caused by infiltration of salinity at transgression. However, the simulated salinity is relatively low compared to measured value at the upper part of the Hayama G.

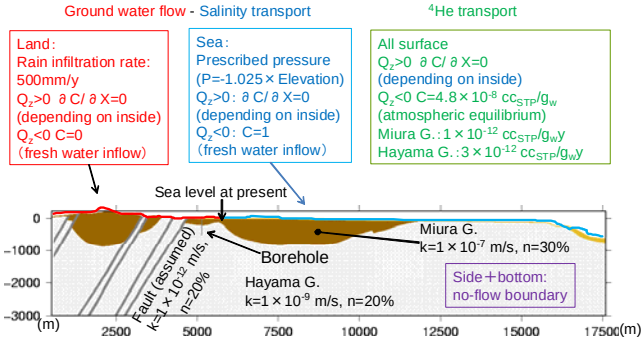

Fig.4 Geological cross-section and boundary conditions.

Sensitive analyses were conducted to prevent washing out salinity at the upper part of the Hayama G. Salinity and ^{4}He distribution could be reproduced by changing hydraulic permeability of fault to that of the Hayama G. Neglecting fault as modeled by hydraulic barrier made groundwater flow from the Hayama G. to the Miura G active. Because fossil sea water supplied from the Hayama G. to the Miura G. This upstream prevents washing out and keeps high salinity and ^{4}He concentration. Hydraulic conductivity of fault is important to reproduce the measured values.

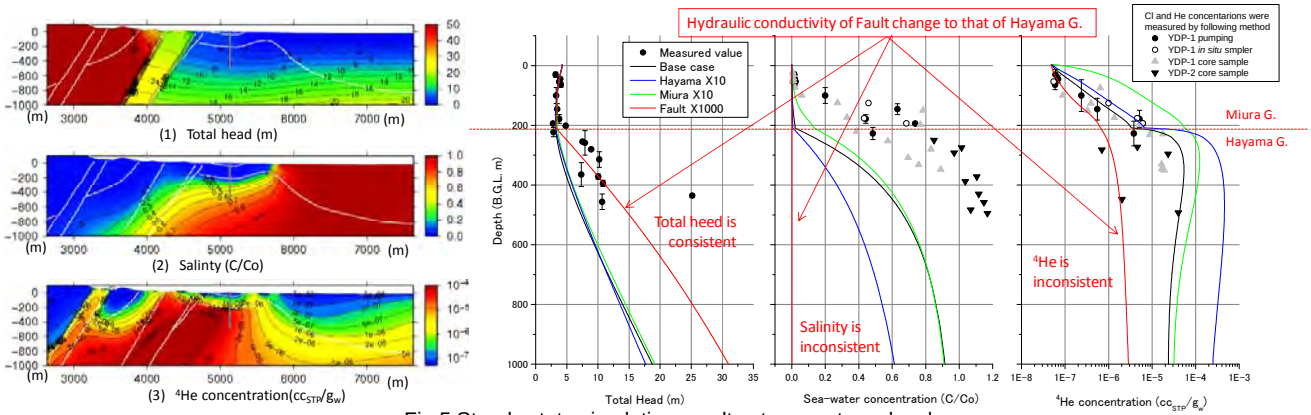

Fig.5 Steady state simulation results at present sea level

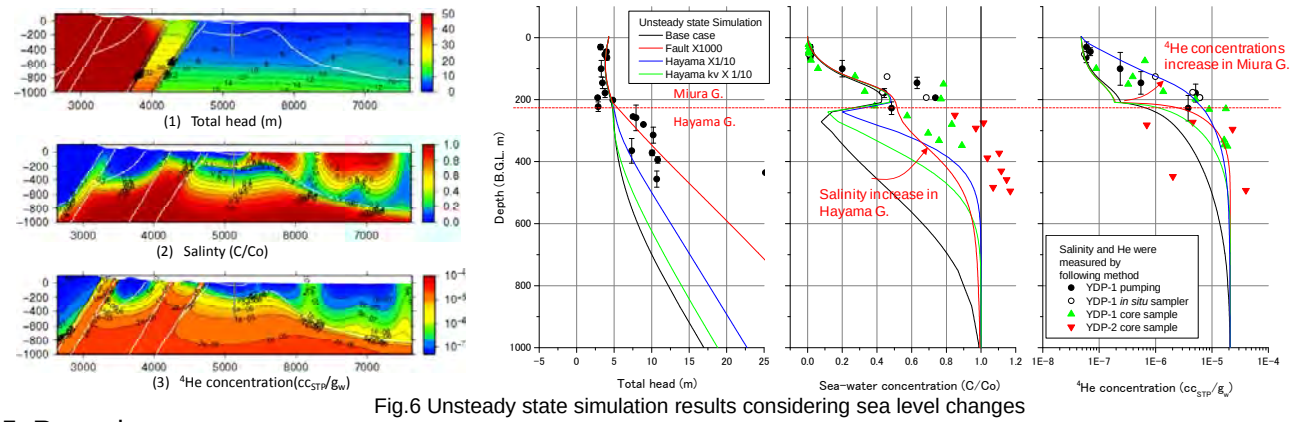

Fig.6 Unsteady state simulation results considering sea level changes

5. Remarks

The conceptual model is integrated as shown in Fig.7.

1) Sea level changes are very important to reproduce,
2) Measured hydraulic conductivities of the Miura G. and the Hayama G. were validated by numerical simulations,
3) Hydraulic conductivity of fault is sensitive to simulation result, and it is confirmed that fault did no act as hydraulic barrier,
4) Groundwater flow from Hayama G. to Miura G. at borehole location is important to reproduce salinity and ^{4}He concentration.

This kind of simulation considering historical influence will be important to predict groundwater flow in the future environment.

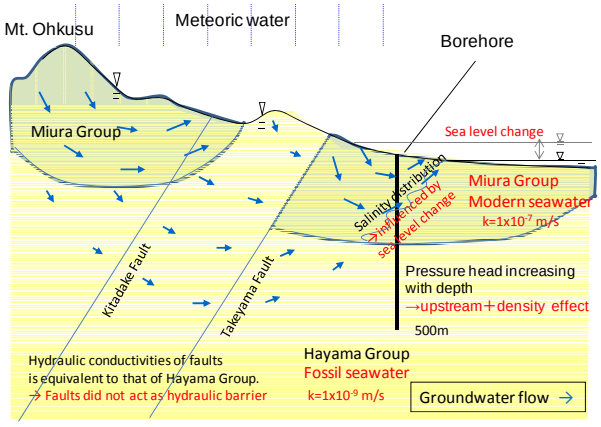

Fig.7 Corrected conceptual groundwater flow model

Acknowledgments

We wish to thank committee members of "Verification of methods for survey and assessment of geological conditions (Chairman; Dr. S. Yoshida)" for their helpful advice for this research.

References

Geological Survey of Japan(2003):Geological Map of Japan 1:1,000,000 3rd Edition, 2nd CD-ROM Version, Geological Survey of Japan,AIST.

Geospatial information Authority of Japan(1997): Digital Map 50m Grid (Elevation),NIPPON-II,CD-ROM.

Hasegawa, T., Nakata,K., Kondo, H., Goto,K., Tomioka Y., Goto,K., Kashiwaya,K.(2011): Identification of modern and fossil sea water using groundwater dating -application of groundwater dating to boring investigation in East costal area of Miura Peninsular-, Report: N10008, CRIEPI.(in Japanese)

Kondo, H., Kiho, K., Goto, K., Hasegawa, T., Hamada, T., Oyama, T., Suzuki, K., Goto. K., Suenaga, H., Nakata, K., Tanaka, S., Nagaoka, T., Kubota, K., Tsuchi,H., Miwa, T., Muramoto, S., Kawano, K., Ito, H.(2011):*Verification study on technology for preliminary investigation –Applicability and issues of methods for borehole drilling and tests in consideration of conditions of geological environment-. Report:N15*, CRIEPI(in Japanese).

Marine Safety Agency(2000):Bathymetric chart(No.6363-1), Basic map of the sea in coastal waters(1:50,000) Uraga Suido, Marine Safety Agency.

Marine Safety Agency(2007):Bathymetric chart(No.6363-5), Basic map of the sea in coastal waters(1:50,000) Sagami Wan,Marine Safety Agency.

J：核種遷移

J.1：Report－Numerical analysis with FEGM/FERM for TRUE-1 non-sorbing tracer tests

ISSN 1104-3210
ISRN SKB-ICR-97/07--SE

NUMERICAL ANALYSIS WITH FEGM/FERM FOR TRUE-1 NON-SORBING TRACER TESTS

Yasuharu Tanaka
Takuma Hasegawa
Motoi Kawanishi

CRIEPI

October 1997

NUMERICAL ANALYSIS WITH FEGM/FERM FOR TRUE-1 NON-SORBING TRACER TESTS

Yasuharu Tanaka
Takuma Hasegawa
Motoi Kawanishi

Abiko Research Laboratory,
Central Research Institute
of Electric Power Industry,
Abiko, Japan

October 1997

Keywords: numerical analysis, tracer test, fracture, pumping, dispersion, transmissivity, drawdown

TABLE OF CONTENTS

EXECUTIVE SUMMARY

The Swedish Nuclear Fuel and Management Company (SKB) planned tracer tests at different experimental scales, the Tracer Retention Understanding Experiments (TRUE) in order to develop the understanding of radionuclide migration and retention in fractured. The basic idea is to perform a series of tracer tests with progressively increasing complexity. The first tracer test cycle (TRUE-1) constitutes a training exercise for tracer test technology on a detailed scale using both non-reactive and reactive tracers in a simple test geometry.

In this study, we performed numerical analyses for the TRUE-1 radially converging tracer test, RC-1, and the TRUE-1 dipole tracer tests, DP 1-4, by using our groundwater and transport models, FEGM/FERM. Groundwater and the tracers were assumed to move only in Feature A. Therefore Feature A was modeled as a single flat square of which the length of the side was 30 meters.

First transimissivities in Feature A were assumed to show a normal distribution in the logarithmic scale and to be distributed spatially with correlation. And the spatial distribution of transmissivity in Feature A was estimated by kriging on basis of the transmissivities at the borehole sections which were identified from drawdowns during the tracer tests. Table 1 and Table 2 give the identified transmissivities at the borehole sections and the drawdowns calculated by using the estimated transmissivity distribution, respectively.

Secondly the hydraulic heads in Feature A under the natural condition were estimated from the hydraulic heads observed at the borehole sections in order to determine the hydraulic boundary conditions. The identified parameters were the hydraulic head at the control point, the magnitude of the average hydraulic gradient and the direction of the average hydraulic gradient.

Thirdly the fluid flux through the tracer injection sections were estimated from the injection concentration curves. The products of the fluid flux and the tracer concentration were used as the mass flux of the tracer injected into Feature A for the tracer migration analysis.

Finally simulations for the tracer migration in Feature A were performed by using the aperture of Feature A and the longitudinal dispersivity as parameters. We could reproduce the experimental breakthrough curves well by computer simulations based on the consistent parameter values, although there were some differences between the calculated results and the experimental ones in a few tracer tests, *see* Figure 1 and Figure 2. From the

results of these simulations, we think that our numerical models, FEGM/FERM, are effective for the analysis of radionuclide migration and retention on a detailed scale in crystalline rock. The following factors are considered to cause the differences. First the input tracer flux in the early stage used in the simulations might be different from the experimental ones because of the measurement errors. Secondly the hydraulic boundary conditions used in the simulations might be different from the ones in the experiments because they were estimated from the hydraulic heads at only five borehole sections. Thirdly the drawdowns calculated by using the estimated spatial distribution of transmissivity in Feature A did not exactly agree with all the observed ones.

Table 1. Transmissivities at borehole sections identified on basis of drawdowns at borehole sections during tracer tests.

Borehole Section	Transmissivity (m^2/s)
KXTT1 R2	9.75×10^{-9}
KXTT2 R2	3.85×10^{-9}
KXTT3 R2	5.00×10^{-2}
KXTT4 R3	2.55×10^{-8}
KA3005A R3	$4.20\times10^{-8*}$

* Not identified but determined from flow- and pressure build-up tests

Table 2. Drawdowns at injection and withdrawal sections calculated by using the estimated spatial distribution of transmissivity in Feature A.

Test#	Injection section		Withdrawal section	
	Observed	Calculated	Observed	Calculated
RC-1			3.1	2.78
DP-1	-4.6	-6.05	1.2	1.35
DP-2	-18	-16.0	40	25.5
DP-3	-5	-5.08	44.5	25.6
DP-4	-15	-16.2	11	11.0

Unit:mH_2O

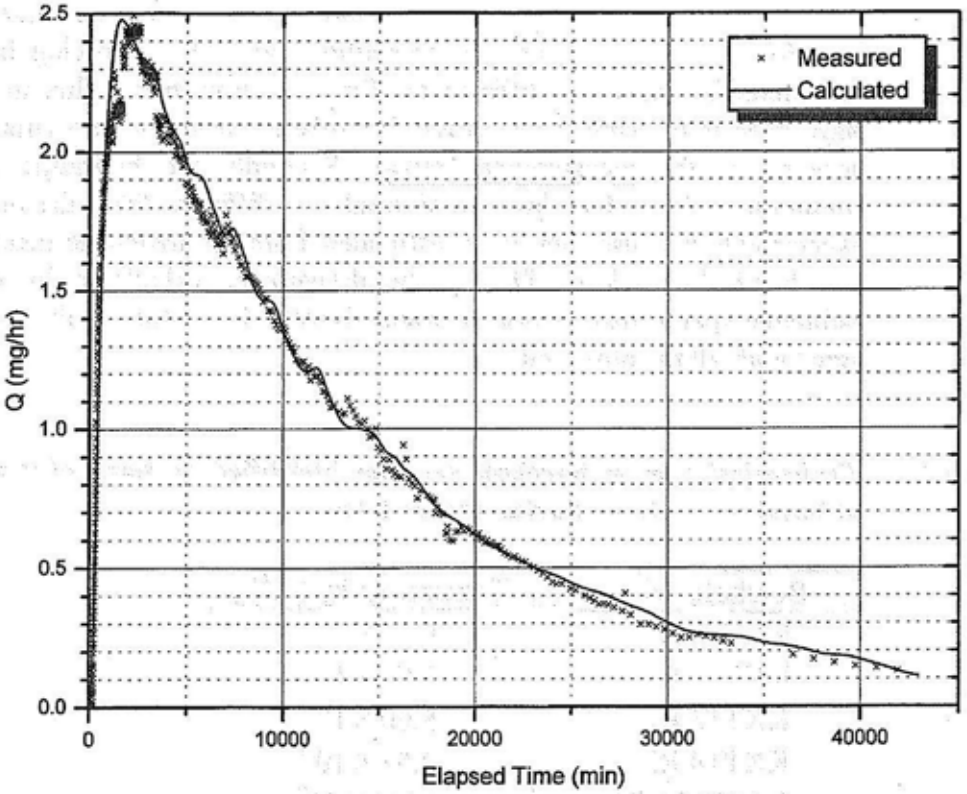

Figure 1. *Simulated and measured breakthrough curves in pumping section of the tracer injected from KXTT4 R3 during RC-1.*

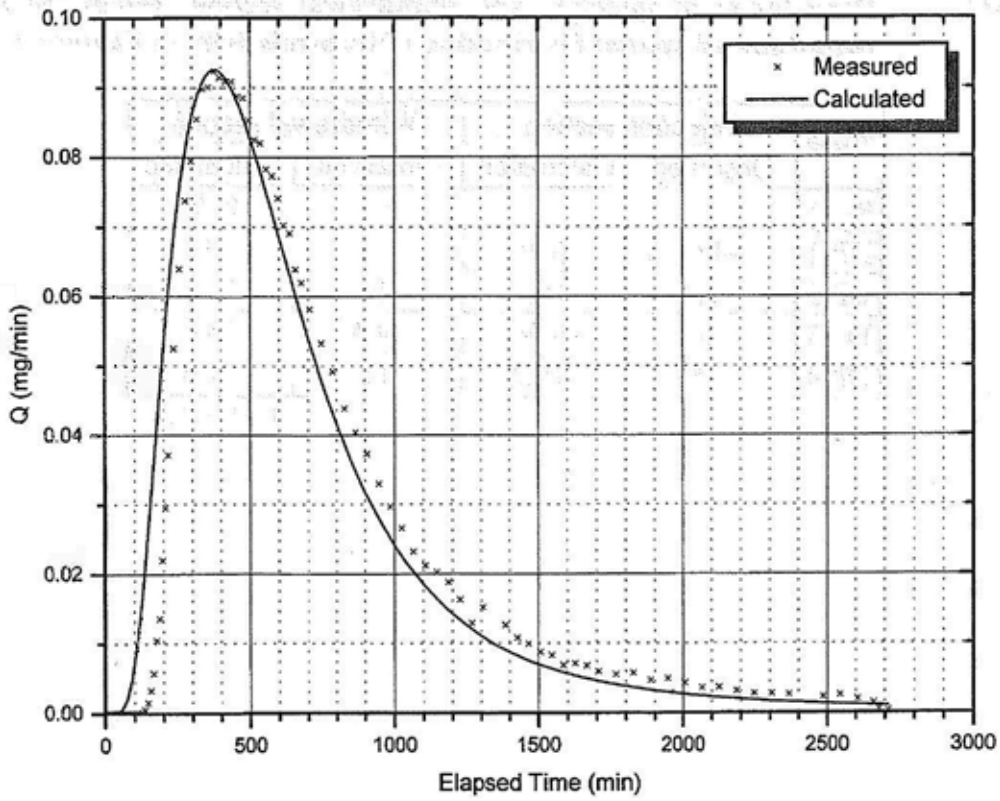

Figure 2. *Simulated and measured breakthrough curves in pumping section during DP-1.*

1. Introduction

The Swedish Nuclear Fuel and Management Company (SKB) is performing various research programs in an underground research laboratory called the Äspö Hard Rock Laboratory to support the design and construction of a deep repository for the high-level nuclear waste. SKB planned tracer tests at different experimental scales, the Tracer Retention Understanding Experiments (TRUE) (Bäckblom and Olsson, 1994). The objectives of the experiments are to develop the understanding of radionuclide migration and retention in fractured rock and to evaluate the usefulness and feasibility of different approaches to model radionuclide migration and retention. The basic idea is to perform a series of tracer tests with progressively increasing complexity.

The first tracer test cycle (TRUE-1) constitutes a training exercise for tracer test technology on a detailed scale using both non-reactive and reactive tracers in a simple test geometry (Winberg, 1996). The TRUE-1 test cycle is expected to contribute data and experience which will constitute the necessary platform for subsequent more elaborate experiments within TRUE at different length scale.

The objectives of the TRUE-1 radially converging tracer test, RC-1, were to determine transport parameters and to test the connectivity of a selected hydraulic feature, Feature A, at the TRUE-1 site within the Äspö HRL. The test was also made to test techniques, tracers and equipment for injection and sampling of tracers in low transmissive rocks for future stage in the TRUE project. The test was performed with pumping in borehole section KXTT3 R2 and injecting in all other (four) borehole sections penetrating Feature A; KXTT1 R2, KXTT4 R3, KXTT2 R2 and KA3005A R3, *see* Figure 1-1. This geometry involved travel distances between 4.7 to 9.6 m. Two tracers, one fluorescent dye and one metal complex, were injected in each section using a decaying pulse injection. Tracer breakthrough from all four injections was monitored in KXTT3 R2. However, at the initially chosen withdrawal rate (0.200 l/min) only two breakthroughs were observed, from the two closest boreholes, KXTT1 R2 and KXTT4 R3 (Andersson, 1996). After increasing the withdrawal rate in two steps, 0.400 and 3 l/min, the tracer injected in other two sections also arrived.

The objectives of the TRUE-1 dipole tracer tests, DP 1-4, were firstly to test the methodology and equipment in low transmissive features, secondly to compare results with the previously performed preliminary tracer tests and the radially converging tracer test and finally to increase the understanding of properties of Feature A and boundary conditions affecting transport in Feature A. The tests were performed in Feature A using three different borehole geometries, *see* Figure 1-2. These flow paths involved travel

distances between 2.6 to 5 meters. One fluorescent dye tracer was injected in each test. In DP-1 also a metal complex was added. Tracer breakthrough in the pumping section was monitored during all four dipole tests. The breakthrough curves all shows one distinct peak and much less tailing than during the radially converging test (RC-1) (Andersson *et al.*, 1997). None of the dipole tests gives complete recovery (30-88%) of injected mass.

In this study, we will perform numerical analyses for RC-1 and DP 1-4 by using our developed groundwater and transport models, FEGM/FERM. First the spatial distribution of transmissivity in Feature A will be estimated by kriging from drawdowns observed in the tracer tests. Secondly the average hydraulic gradient under the natural condition will be estimated in order to determine the hydraulic boundary conditions. Thirdly the fluid flux through the tracer injection sections will be estimated from the injection concentration curves in order to calculate the mass flux of the tracers injected into Feature A. Finally simulations for the tracer migration in Feature A will be performed by using the aperture of Feature A and the longitudinal dispersivity as parameters.

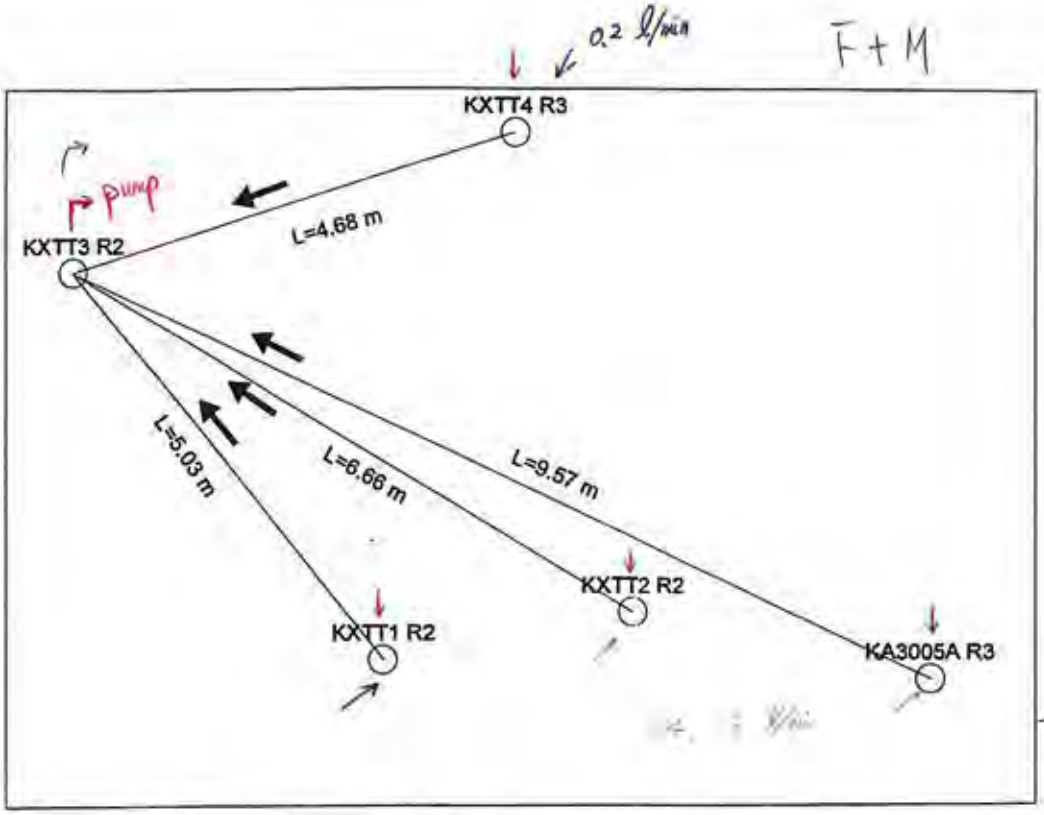

Figure 1-1. *Test geometry for RC-1 and borehole intersection pattern with Feature A (section in the plane of the feature).*

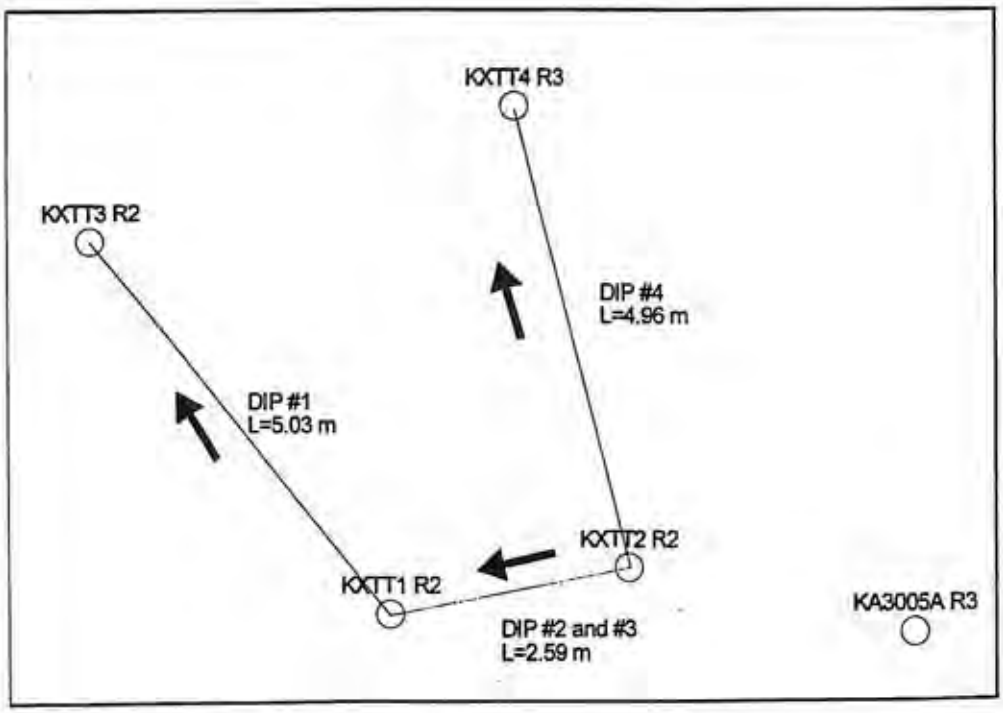

Figure 1-2. *Test geometry for DP 1-4 and borehole intersection pattern with Feature A (section in the plane of the feature).*

2 SIMULATION METHOD

2.1 NUMERICAL MODEL

We applied the groundwater and transport models, FEGM/FERM (Igarashi *et al.*, 1994 and Kawanishi *et al.*, 1987), to this analysis.

The governing equation for groundwater flow is expressed as follows;

$$\frac{\partial}{\partial x_i}\left(T\frac{\partial h}{\partial x_i}\right)+Q=0 \qquad 2\text{-}1$$

where T is the transmissivity, h the hydraulic head and Q the sink or source of the fluid.

The governing equation for solute migration is expressed as follows;

$$b\frac{\partial C}{\partial t}+\frac{\partial V_i C}{\partial x_i}-\frac{\partial}{\partial x_i}\left(D_{ij}\frac{\partial C}{\partial x_j}\right)-M=0 \qquad 2\text{-}2$$

where b is the fracture aperture, C the concentration of the solute, V_i the component of the darcian velocity in the direction x_i and M the sink or source of the solute. And D_{ij} is the tensor of dispersion coefficient of which the ij-th component is expressed as follows;

$$D_{ij}=\alpha_T\frac{|V|}{b}\delta_{ij}+(\alpha_L-\alpha_T)\frac{V_iV_j}{b|V|} \qquad 2\text{-}3$$

where α_T is the longitudinal dispersivity, α_L the transverse one, δ_{ij} Kronecker delta and V the darcian velocity vector.

2.2 MODELING OF FEATURE A

In this study, groundwater and the tracers were assumed to move only in Feature A. Therefore Feature A was modeled as a single flat square of which the length of the side was 30 meters. Figure 2-1 shows the finite element mesh used in the analysis. All the elements are quadrilateral. The total numbers of elements and nodes are 3,855 and 3,955 respectively. The

boreholes were expressed as cavities.

The hydraulic heads were fixed on the surrounding boundaries of the model and no flux of the tracers were assumed to cross the boundaries. The time-varying mass flux of the tracers was prescribed at the injection boreholes.

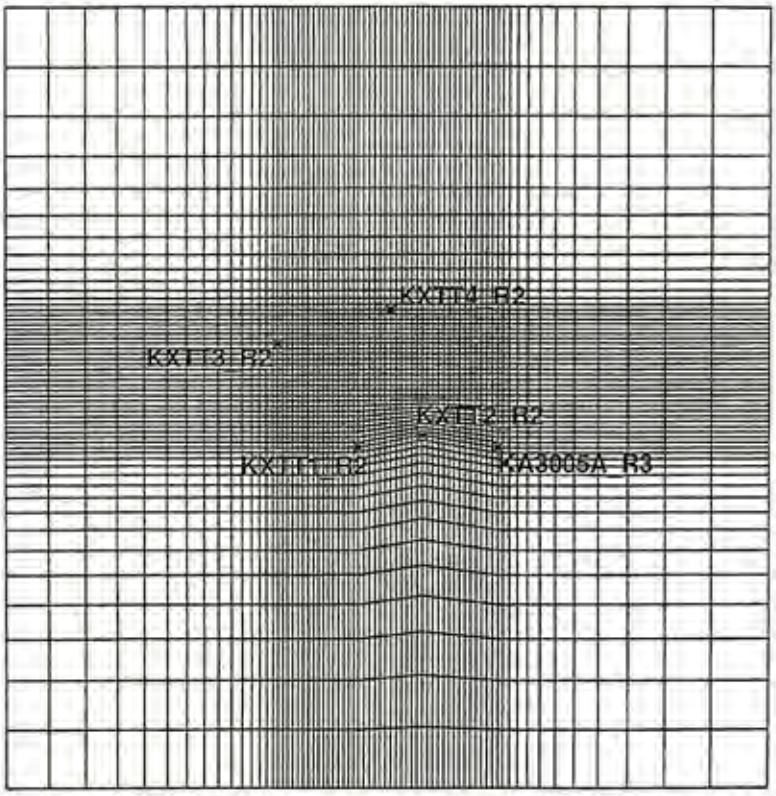

30m×30m
3,855 elements 3,955 nodes

Figure 2-1. *Finite element mesh for the numerical analysis.*

2.3 TRANSMISSIVITY IN FEATURE A

Transimissivities in Feature A were assumed to show a normal distribution in the logarithmic scale and to be distributed spatially with correlation. The spatial distribution of the transmissivity in Feature A was estimated by kriging on the basis of the transmissivities at the five borehole sections.

By kriging method, the estimation at the point x, T^*, can be obtained as the linear sum of the values at the measurement point x_i, T_i (de Marsily, 1986).

$$T^*(x)=\sum_{i=1}^{n}\lambda^i(x)\cdot T_i \qquad 2\text{-}4$$

where n is the number of the measurement points and $\lambda_i(x)$ the weights of the kriging estimator. The following condition is required in order to have an unbiased estimator.

$$\sum_i \lambda^i(x)=1 \qquad 2\text{-}5$$

And the errors of estimation must be minimal so that the estimator is optimal.

$$E\left[\left\{T^*(x)-T(x)\right\}^2\right] \text{ minimum} \qquad 2\text{-}6$$

where E represents the expectation of the value in parenthesis. The values of $\lambda_i(\mathbf{x})$ which satisfy the conditions 2-5 and 2-6 can be obtained by solving the following simultaneous equations.

$$\begin{aligned}&\sum_j \lambda^j(x)\gamma(x_i-x_j)+\mu=\gamma(x_i-x_0) \quad i=1,\cdots,n\\&\sum_i \lambda^i(x)=1\end{aligned} \qquad 2\text{-}7$$

where μ is an unknown, called a Lagrange multiplier. And γ is the variogram defined by the following equation.

$$\gamma(h)=\frac{1}{2}\text{var}[Y(x+h)-Y(x)] \qquad 2\text{-}8$$

where var represents the variance of the value in parenthesis. In this study, the following exponential model was used to express variogram.

$$\gamma(h) = \sigma^2 \cdot \left\{1 - exp\left(-\frac{h}{a}\right)\right\} \qquad 2\text{-}9$$

where σ^2 is the variance of the logarithmic transmissivity, h the distance and a the correlation length.

3 SIMULATED RESULTS

3.1 TRANSMISSIVITY IN FEATURE A

The transmissivities at all the borehole sections except for KA3005A R3 were identified so that the sum of the squares of normalized errors between the calculated drawdowns and the observed ones, S_d, would be minimal.

$$S_d = \sum_{i=1}^{9} \left(\frac{\Delta h^i_{cal} - \Delta h^i_{obs}}{\Delta h^i_{obs}} \right)^2 \qquad 3\text{-}1$$

where Δh^i_{obs} is the i-th observed drawdown at the withdrawal or injection section. And Δh^i_{cal} is the i-th drawdown calculated by using the spatial distribution of transimissivity in Feature A which is estimated by kriging on basis of the transmissivities at the five borehole sections. In the kriging estimation, the correlation length was assumed to be 1 meter and the value determined from the flow- and pressure build-up test (Winberg, 1996) was used as the transmissivity at KA3005A R3. The identified transmissivities are given in Table 3-1. And Figure 3-1 shows the spatial distribution of transmissivity in Feature A estimated on basis of the identified section transmissivities. The estimated transmissivities at the points distant from the borehole sections are almost uniform because they are hardly correlated with the transmissivities at the borehole sections. The drawdowns calculated by using the estimated transmissivity distribution are given in Table 3-2. In this study, we used this estimated transmissivity distribution as the spatial distribution of transmissivity in Feature A.

3.2 HYDRAULIC BOUNDARY CONDITION

The hydraulic heads were fixed on the surrounding boundaries of the model as mentioned in 2.2. The hydraulic heads on the boundaries were identified so that the sum of the squares of normalized errors between the calculated heads and the observed ones at the five borehole sections under the natural condition, S_h, would be minimal.

$$S_h = \sum_{i=1}^{5} \left(\frac{h^i_{cal} - h^i_{obs}}{h^i_{obs}} \right)^2 \qquad 3\text{-}2$$

where h^i_{obs} is the observed hydraulic head at the i-th section under the

natural condition and h^i_{cal} the calculated one. The identified parameters were the hydraulic head at the point A, h_A, the magnitude of the average hydraulic gradient, I, and the angle between the direction of the average hydraulic gradient and the side AB, θ, *see* Figure 3-2. Table 3-3 gives the identified values of these parameters for RC-1 and DP 1-4.

3.3 MASS FLUX AT INJECTION SECTION

The fluid flux through the tracer injection section, Q_{bh}, is obtained theoretically by the following equation (Winberg, 1996 and Andersson, 1996).

$$Q_{bh} = -\frac{V}{t} ln(C/C_0) - Q_{sam} \qquad 3\text{-}3$$

where V is the volume of the tracer injection section, t the elapsed time, C_0 the initial concentration of the tracer in the injection section, C the concentration at the time t and Q_{sam} the sampling flow rate. The measured values of the tracer concentration and the straight line for approximation are shown in Figure 3-3 - Figure 3-8. The fluid flux through the tracer injection sections was calculated by using the equation 3-3 from the slope of the straight line. Table 3-4 gives the calculated flux.

The product of the tracer concentration and the fluid flux was used as the mass flux of the tracer injected into Feature A for the tracer migration analysis.

3.4 TRACER MIGRATION ANALYSIS

Simulations for the tracer migration in Feature A were performed on basis of the above-mentioned conditions. The aperture of Feature A, b, and the longitudinal dispersivity, α_L, were estimated through the simulations. The ratio of longitudinal dispersivity to transverse one was fixed at 10:1 in the simulations.

The best-fit runs are shown in Figure 3-9 - Figure 3-14 and the estimated values of parameters are given in Table 3-5. Differences in the estimated aperture between the tests correspond to the heterogeneity of aperture in Feature A. The tracer travel times, t_5, t_{50} and t_{95}, defined as times when 5, 50 and 95 % of the recovered mass respectively had arrived are given in Table 3-6. The tracer recoveries at the end of the tests are given in Table 3-7.

RC-1 : the tracer injected from KXTT1 R2
The calculated breakthrough curve in the pumping section agrees well with the measured one before the time when the flux of the tracer is the largest. However after that time the calculated breakthrough curve is behind the

measured one.

RC-1 : the tracer injected from KXTT4 R3
The calculated breakthrough curve almost agrees with the measured one, although the calculated one reaches its peak earlier than the measured one.

DP-1
The calculated largest flux of the tracer and the time when the calculated flux is the largest are in good agreement with the measured results. But the calculated flux is larger than the measured one before the peak time while the calculated one is smaller than the measured one after that time.

DP-2
The time when the calculated flux of the tracer is the largest agrees with the measured one. But the calculated flux of the tracer is slightly larger than the measured one through the period of experimentation and the calculated peak flux is larger than the measured one by 5%.

DP-3
The time when the calculated flux of the tracer is the largest agrees with the measured one. But the calculated flux of the tracer is larger than the measured one through the period of experimentation and the calculated peak flux is larger than the measured one by 15%.

DP-4
The time when the calculated flux of the tracer is the largest agrees with the measured one. But the calculated flux of the tracer is larger than the measured one through the period of experimentation and the calculated peak flux is larger than the measured one by 20%.

We think that we could reproduce the experimental breakthrough curves well by computer simulations based on the consistent parameter values although there were some differences between the calculated results and the experimental ones in a few tracer tests. The following factors are considered to cause the differences. First the concentration values measured in the injection sections in the early stage of the experiments were not accurate due to delay and dispersion in the sampling line (Andersson, 1996). Accordingly the input tracer flux in the early stage used in the simulations might be different from the ones in the experiments. Secondly the natural hydraulic gradient was estimated on basis of the hydraulic heads at only five borehole sections. So the hydraulic boundary conditions used in the simulations might be different from the ones in the experiments. Thirdly the transmissivities at the five borehole sections were identified so that they would satisfy the drawdowns observed in all the tracer tests properly at the same time. Consequently the calculated drawdowns did not exactly agree with all the observed ones, *see* Table 3-2.

Table 3-1. Transmissivities at borehole sections identified on basis of drawdowns at borehole sections during tracer tests.

Borehole Section	Transmissivity (m^2/s)
KXTT1 R2	9.75×10^{-9}
KXTT2 R2	3.85×10^{-9}
KXTT3 R2	5.00×10^{-2}
KXTT4 R3	2.55×10^{-8}
KA3005A R3	$4.20\times10^{-8*}$

* Not identified but determined from flow- and pressure build-up tests

Table 3-2. Drawdowns at injection and withdrawal sections calculated by using the estimated spatial distribution of transmissivity in Feature A.

Test#	Injection section		Withdrawal section	
	Observed	Calculated	Observed	Calculated
RC-1			3.1	2.78
DP-1	-4.6	-6.05	1.2	1.35
DP-2	-18	-16.0	40	25.5
DP-3	-5	-5.08	44.5	25.6
DP-4	-15	-16.2	11	11.0

Unit:mH_2O

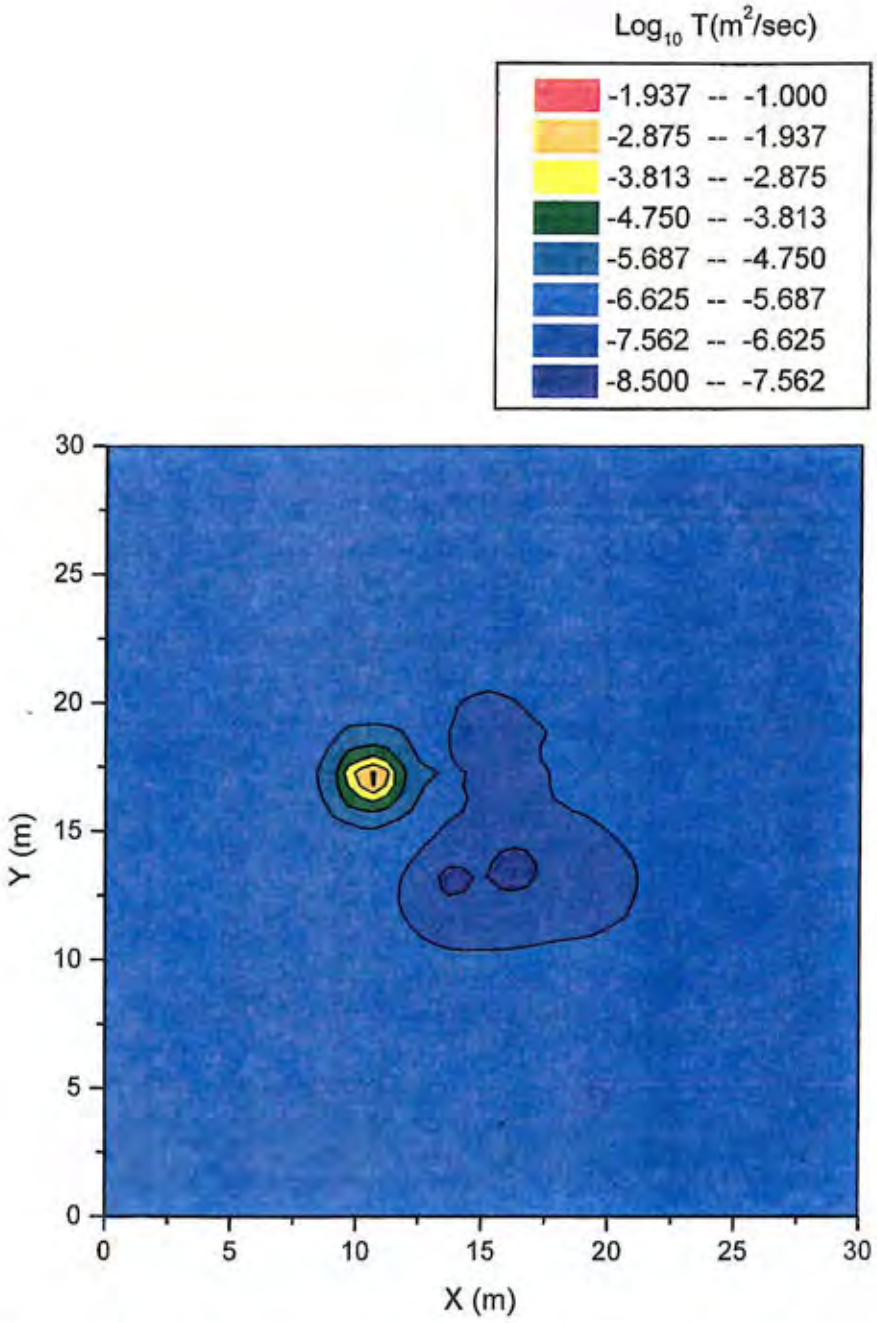

Figure 3-1.*Spatial distribution of logarithmic transmissivitiy in Feature A estimated by kriging on basis of the identified transmissivities at the five borehole sections. (KXTT1 R2:(X,Y)=(13.78, 13.04), KXTT2 R2:(16.32, 13.53), KXTT3 R2:(10.63, 17.04), KXTT4 R3:(15.06, 18.35), KA3005A R3:(19.22, 13.03))*

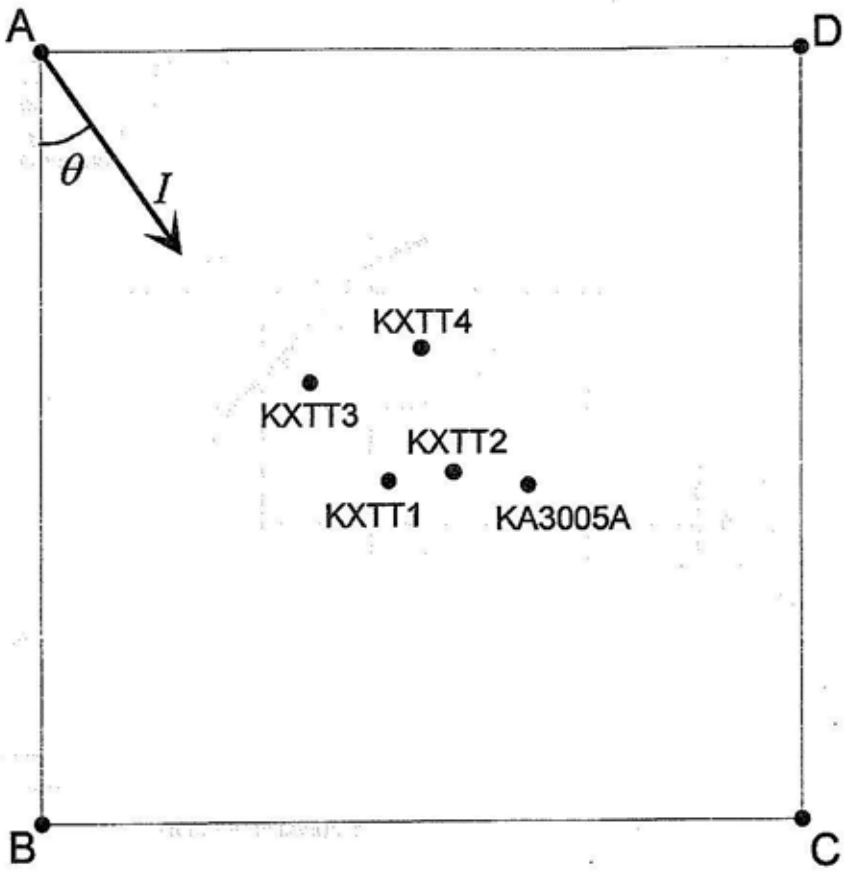

Figure 3-2. Schematic diagram for parameters defining hydraulic boundary conditions.

Table 3-3. Identified values of parameters for hydraulic boundary conditions.

Parameters	RC-1	DP-1～4
Hydraulic head, h_A	-45.7mH_2O	-47.9mH_2O
Magnitude of hydraulic gradient, I	0.0858	0.140
Direction of hydraulic gradient, θ	46. 5°	68.5°

Table 3-4. Fluid flux calculated on basis of tracer concentration in injection sections.

Test #	Injection section	Q_{bh} (ml/min)	Remarks
RC-1	KXTT1 R2	0.102	t<318.16min
		0.230	t>318.16min
	KXTT4 R3	0.118	
DP-1	KXTT1 R2	9.88	
DP-2	KXTT2 R2	9.78	
DP-3	KXTT2 R2	3.58	
DP-4	KXTT2 R2	9.73	t<1200min
		2.81	t>1200min

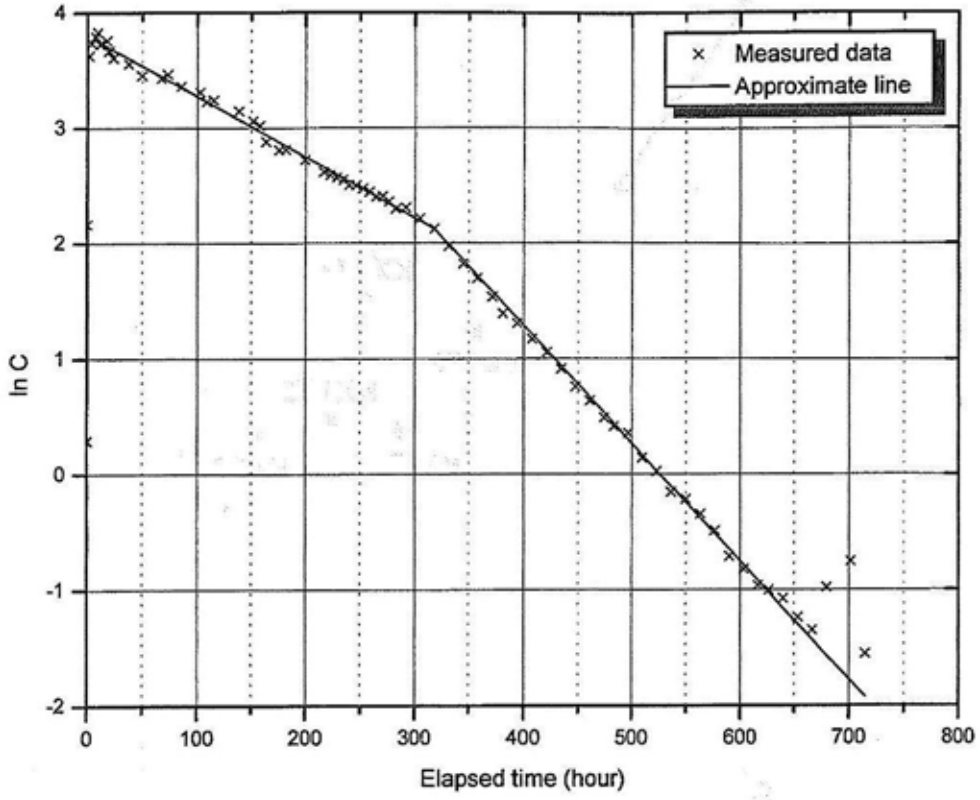

Figure 3-3. *Injected tracer concentration (ln C) in KXTT1 R2 during RC-1.*

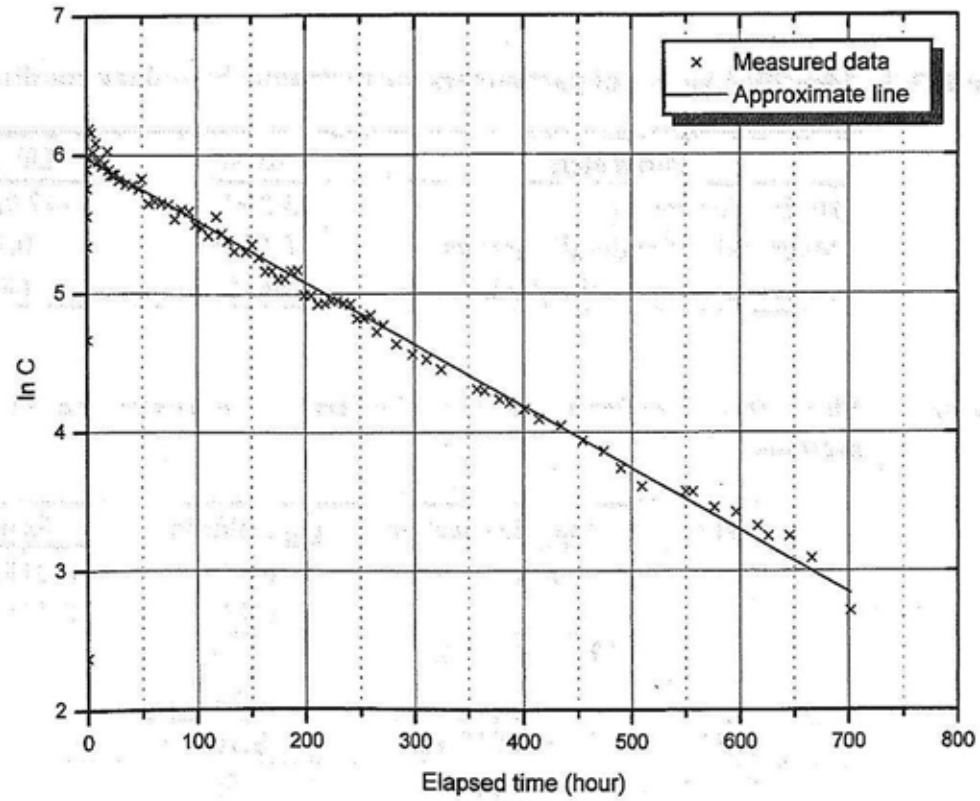

Figure 3-4. *Injected tracer concentration (ln C) in KXTT4 R3 during RC-1.*

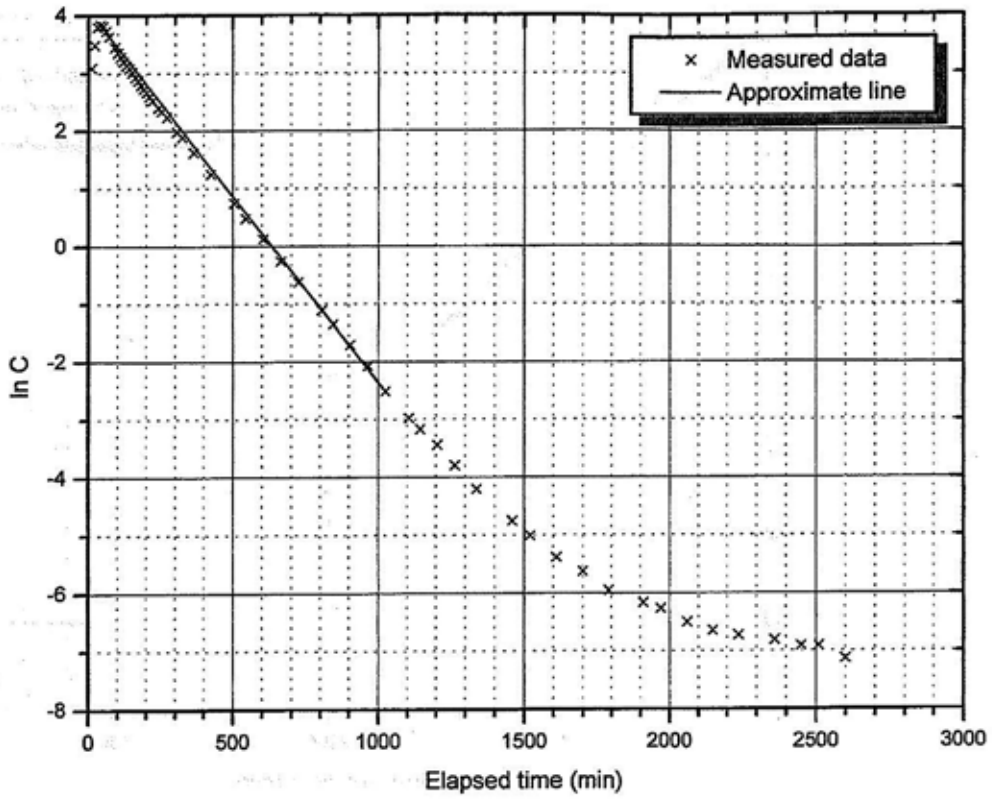

Figure 3-5. *Injected tracer concentration (ln C) in KXTT1 R2 during DP-1.*

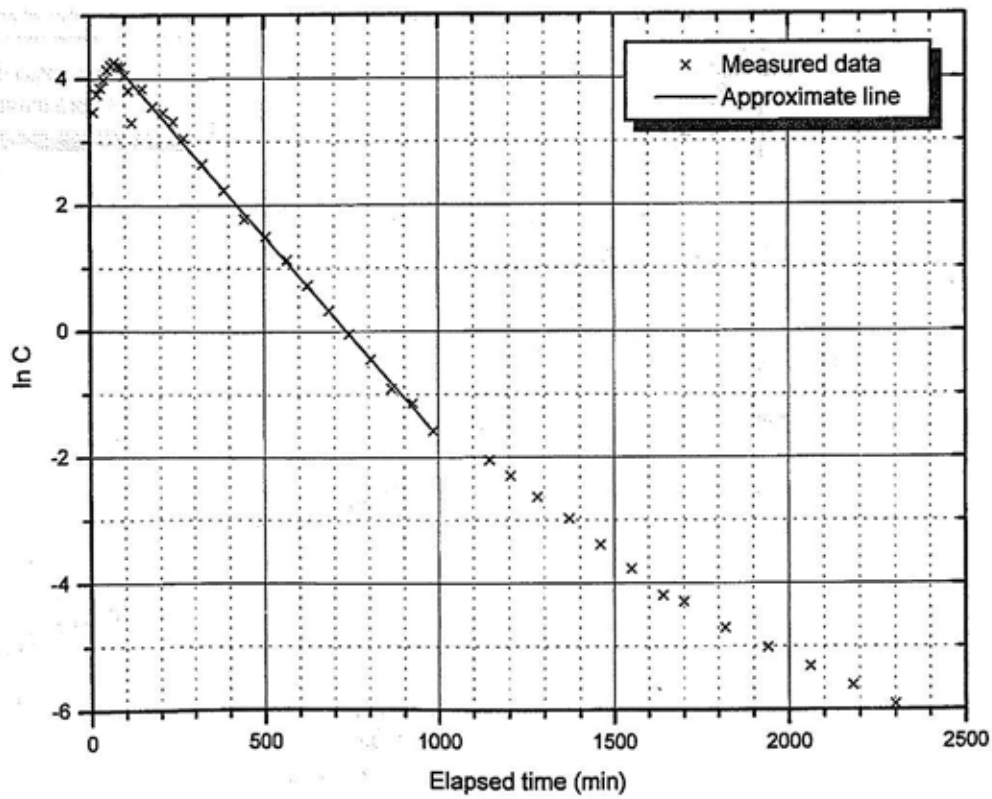

Figure 3-6. *Injected tracer concentration (ln C) in KXTT2 R2 during DP-2.*

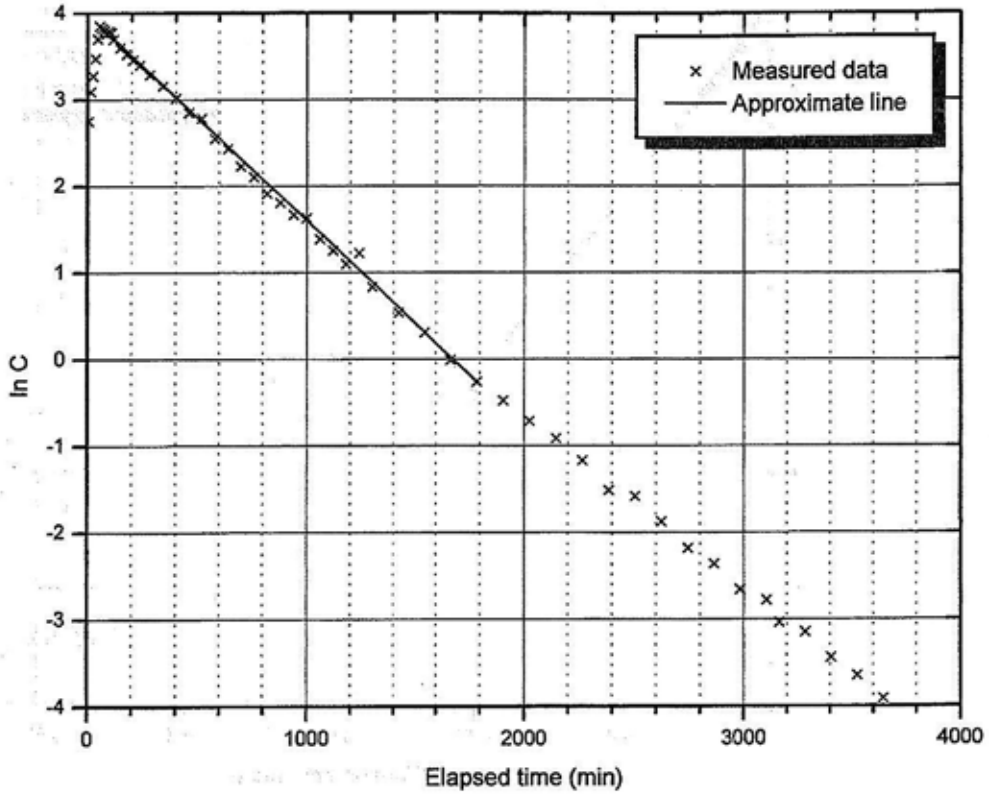

Figure 3-7. *Injected tracer concentration (ln C) in KXTT2 R2 during DP-3.*

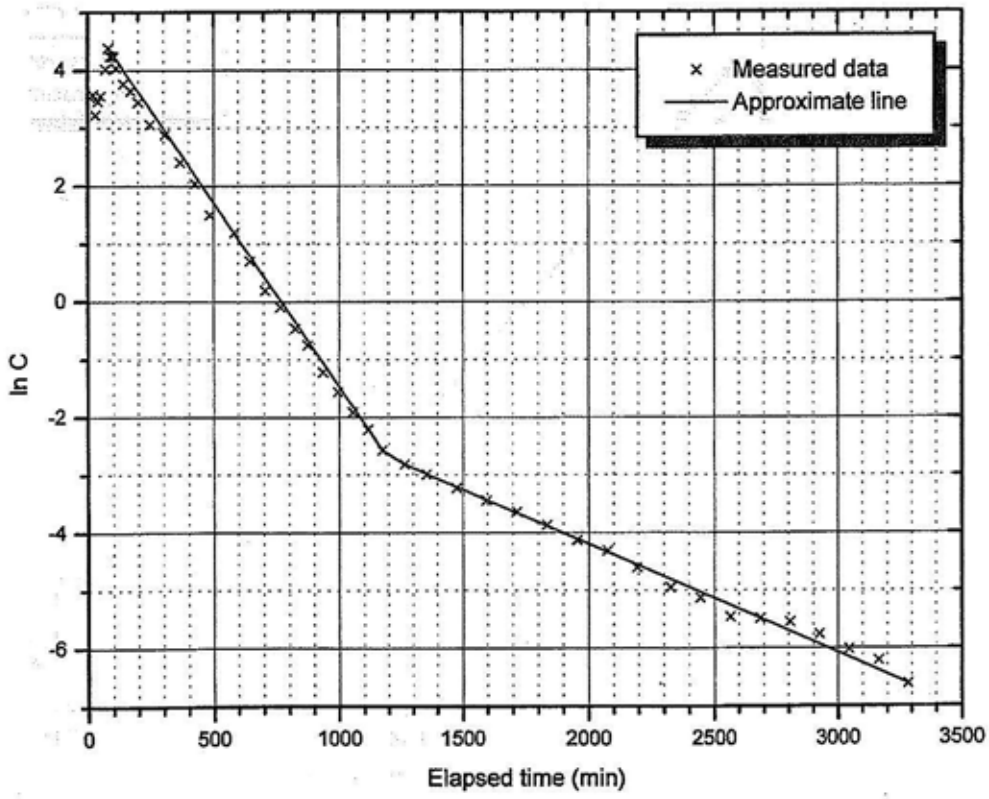

Figure 3-8. *Injected tracer concentration (ln C) in KXTT2 R2 during DP-4.*

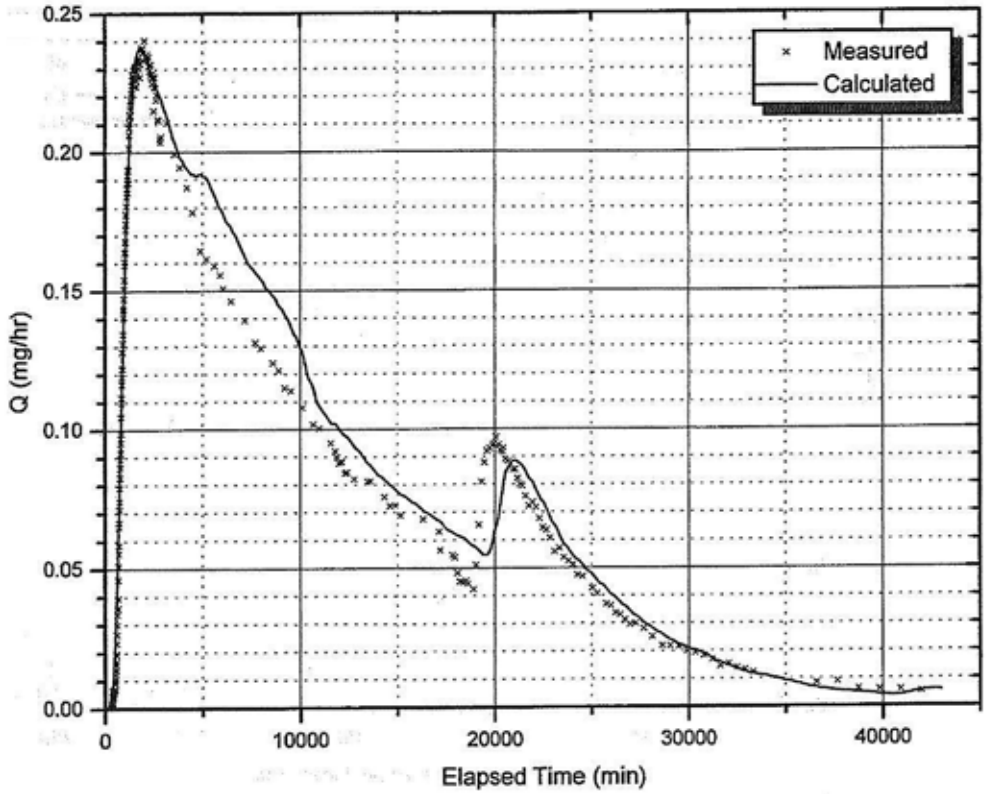

Figure 3-9. *Simulated and measured breakthrough curves in pumping section of the tracer injected from KXTT1 R2 during RC-1.*

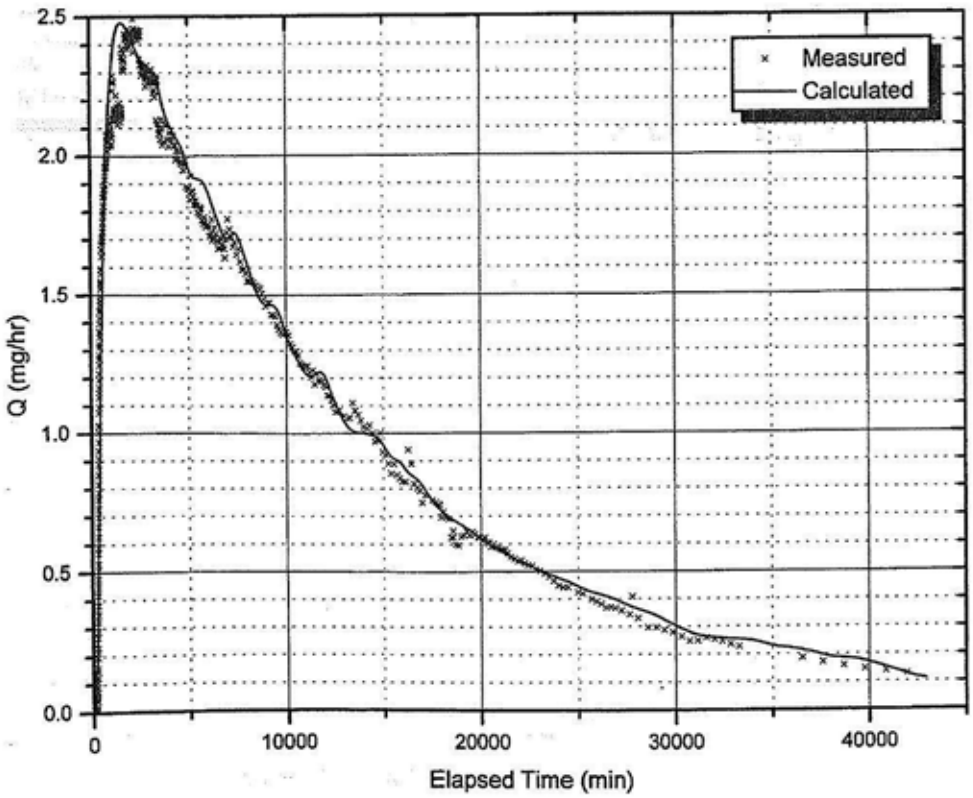

Figure 3-10. *Simulated and measured breakthrough curves in pumping section of the tracer injected from KXTT4 R3 during RC-1.*

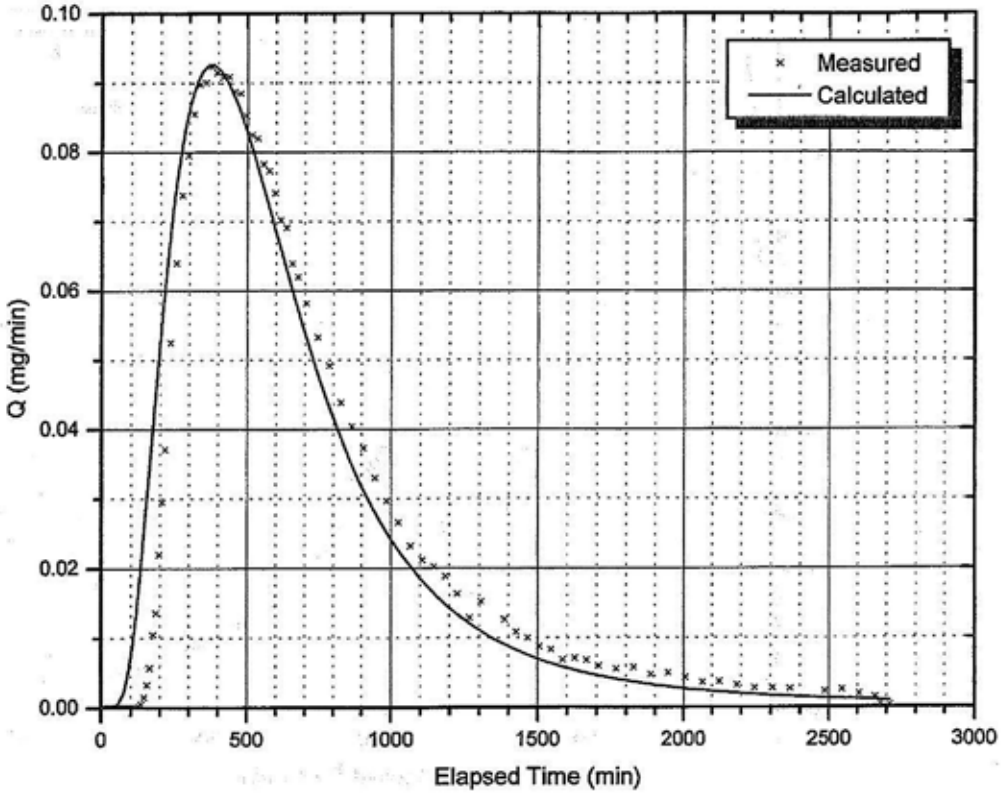

Figure 3-11. *Simulated and measured breakthrough curves in pumping section during DP-1.*

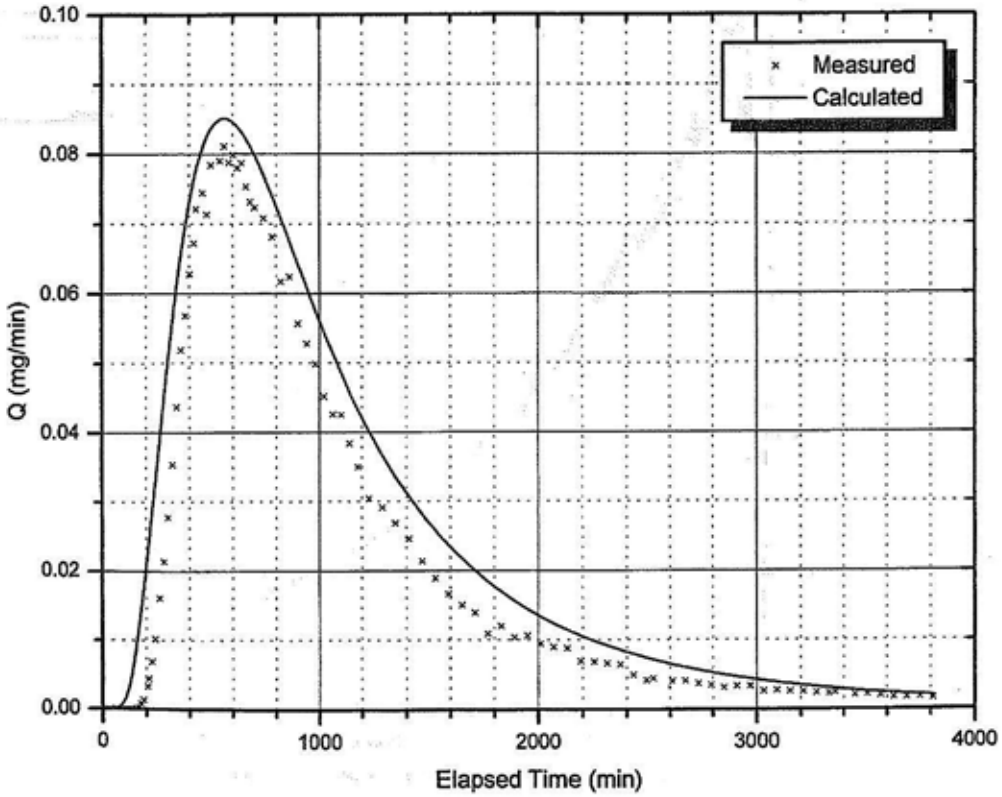

Figure 3-12. *Simulated and measured breakthrough curves in pumping section during DP-2.*

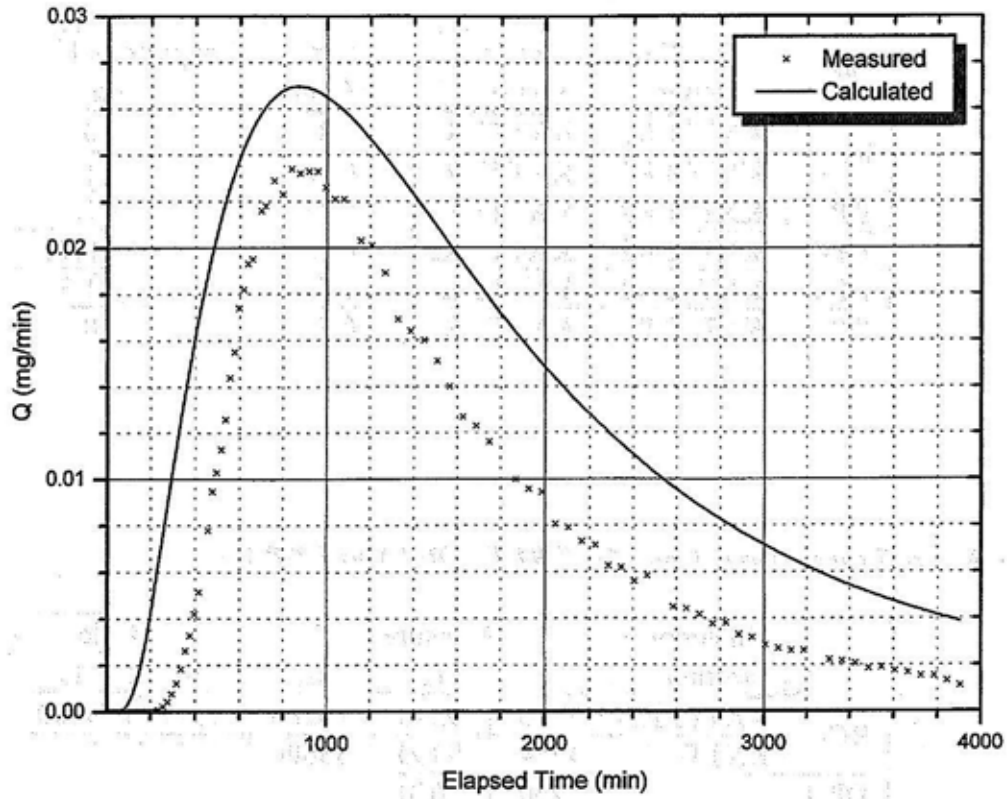

Figure 3-13. *Simulated and measured breakthrough curves in pumping section during DP-3.*

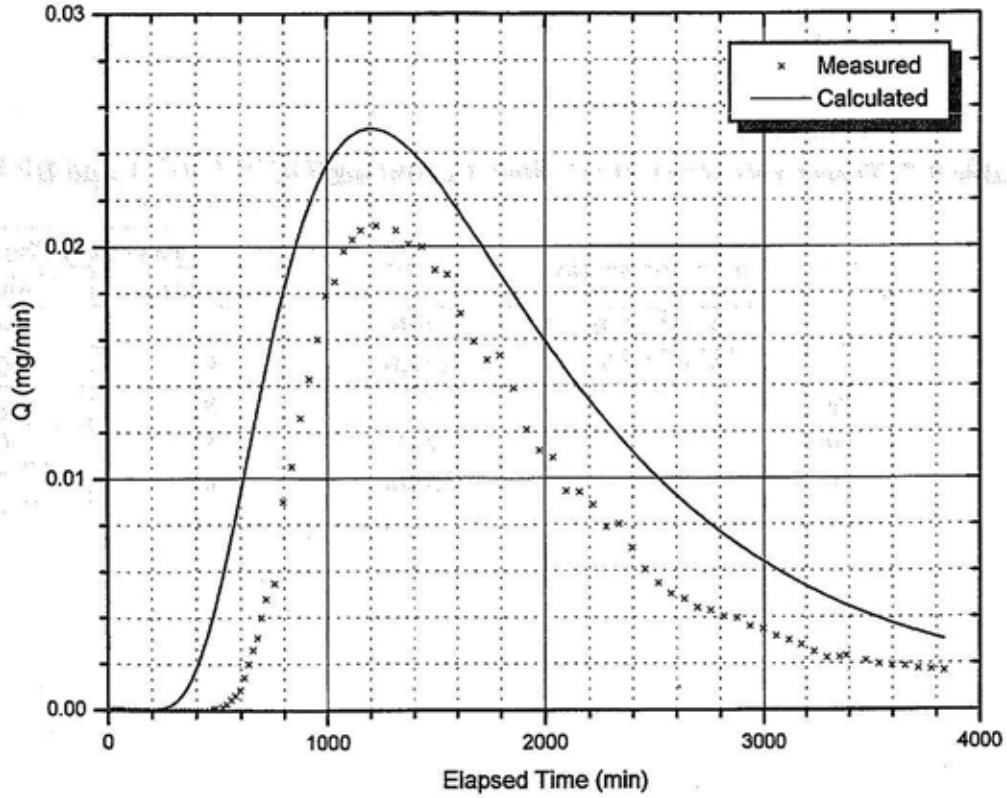

Figure 3-14. *Simulated and measured breakthrough curves in pumping section during DP-4.*

Table 3-5. Best fit parameters for breakthrough curves in withdrawal sections.

Test #	Injection section	Withdrawal section	Aperture b (mm)	Longitudinal Dispersivity α_L (m)
RC-1	KXTT1 R2	KXTT3 R2	0.33	0.19
	KXTT4 R3	KXTT3 R2	0.52	1.00
DP-1	KXTT1 R2	KXTT3 R2	0.23	1.10
DP-2	KXTT2 R2	KXTT1 R2	0.75	0.71
DP-3	KXTT2 R2	KXTT1 R2	0.71	1.37
DP-4	KXTT2 R2	KXTT4 R3	0.51	0.95

Table 3-6. Tracer travel times for TRUE-1 RC-1 and DP 1-4.

Test #	Injection section	Measured			Calculated		
		t_5	t_{50}	t_{95}	t_5	t_{50}	t_{95}
RC-1	KXTT1 R2	1530	9240	29280	1571	9100	28318
	KXTT4 R3	1254	9360	33600	1270	9336	33527
DP-1		260	620	2220	204	544	1531
DP-2		362	845	2560	306	870	2554
DP-3		556	1272	3070	423	1393	3340
DP-4		856	1563	3150	693	1581	3271

Unit : min

Table 3-7. Tracer recoveries at the time, t_{100}, during TRUE-1 RC-1 and DP 1-4.

Test #	Injection section	t_{100} (min)	Recovery (%)	
			Measured	Calculated
RC-1	KXTT1 R2	43004	91	99.5
	KXTT4 R3	42944	97	99.3
DP-1		2711	88	81.6
DP-2		3811	56	68.0
DP-3		3906	45	70.9
DP-4		3836	30	32.9

4 CONCLUSIONS

A numerical analysis was performed for the TRUE-1 radially converging tracer test, RC-1, and the dipole tracer tests, DP 1-4. Our developed groundwater and transport models, FEGM/FERM were applied to the analysis.

In this study, groundwater and the tracers were assumed to move only in Feature A. Consequently Feature A was modeled as a single flat square of which the length of the side was 30 meters.

First the transmissivities at all the borehole sections except for KA3005A R3 were identified from the drawdowns observed during the tracer tests. The spatial distribution of transmissivity in Feature A was estimated by kriging on basis of the identified section transmissivities. Secondly the average hydraulic gradient under the natural condition was identified from the hydraulic heads at the five borehole sections. The hydraulic conditions on the surrounding boundaries were determined on basis of the natural hydraulic gradient. Thirdly the fluid flux through the tracer injection sections was estimated from the injection concentration curves in order to calculate the mass flux of the tracers injected into Feature A. Finally simulations for the tracer migration in Feature A were performed by using the aperture of Feature A and the longitudinal dispersivity as parameters.

We could reproduce the experimental breakthrough curves well by computer simulations based on the consistent parameter values, although there were some differences between the calculated results and the experimental ones in a few tracer tests. From the results of these simulations, we think that our numerical models, FEGM/FERM, are effective for the analysis of radionuclide migration and retention on a detailed scale in crystalline rock. The following factors are considered to cause the differences. First the input tracer flux in the early stage used in the simulations might be different from the experimental ones because of the measurement errors. Secondly the hydraulic boundary conditions used in the simulations might be different from the ones in the experiments because they were estimated from the hydraulic heads at only five borehole sections. Thirdly the drawdowns calculated by using the estimated spatial distribution of transmissivity in Feature A did not exactly agree with all the observed ones.

REFERENCES

Bäckblom G, Olsson O, 1994. Program for tracer retention understanding experiments. Swedish Nuclear Fuel and Waste Management. Äspö Hard Rock Laboratory Progress Report PR 25-94-24.

Winberg A, 1996. Descriptive structural-hydraulic models on block and detailed scales of the TRUE-1 site. SKB International Cooperation Report ICR 94-08.

Andersson P, 1996, TRUE 1st stage tracer test program. Experimental data and preliminary evaluation of the TRUE-1 radially converging tracer test (RC-1). Äspö Hard Rock Laboratory Progress Report HRL-96-24.

Andersson P, Nordqvist R, Jönsson S, 1997. TRUE 1st stage tracer test program. Experimental data and preliminary evaluation of the TRUE-1 dipole tracer tests (DP-1 – DP-4). Äspö Hard Rock Laboratory Progress Report HRL-97-13.

Igarashi T, Tanaka Y, Kawanishi M, 1994. Application of three-dimensional smeared fracture model to the groundwater flow and the solute migration of LPT-2 experiment. SKB International Cooperation Report ICR 94-08.

Kawanishi M, Igarashi T, Mahara Y, Komada H, Maki Y, 1987. Computer models for safety assessment on land disposal of low-level wastes. Waste Management '87, 3, Tucson, Arizona, pp. 175-180.

de Marsily G, 1986. Quantitative Hydrogeology. Academic Press, INC..

J.2：Paper－Clarification of Requirements for Hydraulic Conductives of Backfill and Plug Materials in HLW Disposal Systems

Clarification of Requirements for Hydraulic Conductivities of Backfill and Plug Materials in HLW Disposal Systems

Y. Tanaka
Central Research Institute of Electric Power Industry
1646 Abiko, Abiko-shi, Chiba-ken 270-1194, JAPAN

R. Masuda
Tokyo Electric Power Company
1-3 Uchisaiwai-cho 1-chome Chiyoda-ku, Tokyo 100-0011, JAPAN

K. Ando
Obayashi Corporation
Shinagawa Intercity Tower B, 2-15-2, Konan, Minato-ku, Tokyo 108-8502, JAPAN

1. Introduction

Several shafts are planned for the transport of waste packages and various instruments and to change the air in a geological disposal facility for high-level radioactive wastes. In our safety assessment on the geological disposal of high-level radioactive wastes, we suppose that the radionuclides leaking from the engineered barrier system migrate through the natural barrier, that is, the rock matrix to the biosphere. Therefore, it is vital to take measures so that the shafts will not become the critical path for migration of radionuclides.

So far, we have supposed that the emplacement tunnels are backfill so as to have hydraulic conductivity as low as the surrounding rock matrix. According to our preliminary design, the total length of the emplacement tunnels will be over 200 kilometers in the vertical emplacement concept in depth of about 500m. Therefore, the requirement of the material backfilliing the emplacement tunnels will significantly influence the total cost for the construction of a geological disposal facility.

In this study, we tried to clarify the requirements for the hydraulic conductivities of the backfill and plug materials in a Japanese geological disposal system of high-level radioactive wastes by groundwater flow and solute transport analyses.

2. Hydraulic requirements for backfill and plug materials in shaft

2.1 Investigation method

We suppose that the HLW disposal facility is to be built in the center of an impervious geological formation 200 meters thick and hydraulic plugs are installed within 100 meters upward from the bottom of the shafts.

A two-dimensional axis-symmetric model with respect to the centerline of a shaft was used for the numerical analysis. The numerical model is shown in Figure 1. The size of the model domain is 140 meters in the vertical direction and 50 meters in the radial direction. The diameter of the shaft is 7 meters. The

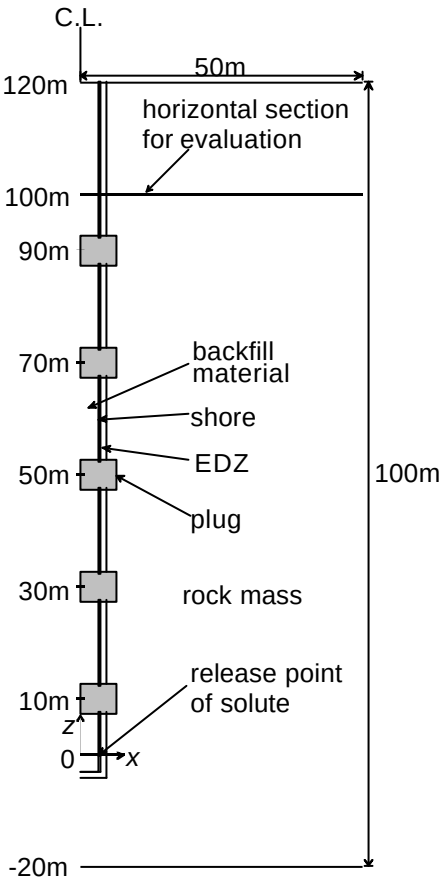

Figure 1. Numerical model used in the analysis for shaft

shaft is connected to the access tunnel at its bottom and the origin of the coordinate system is set at the intersection of the centerlines of the access tunnel and the shaft. The diameter of the access tunnel is 6.5 meters. The concrete lining with a 0.25 meter thickness is built on the inside of the shaft and the access tunnel in the sedimentary rock concept. On the other hand, there is no lining in the granitic rock concept. The candidate positions for setting plugs are z = 10, 30, 50, 70 and 90 m as the center of the plugs. The diameter and height of the plugs are from 9 to 15 meters and 5 meters, respectively. The excavation-disturbed zone with a 1 meter thickness was assumed to exist around the shaft and the access tunnel according to experimental data published in literature (Frieg *et al*., 1996). No excavation-disturbed zone around the plugs was assumed, because the rock mass around the plugs is expected to be excavated very carefully by electric saws, etc. so as not to generate an excavation-disturbed zone and a reduction of hydraulic conductivity by the skin effect is possible.

As the hydraulic boundary conditions, hydraulic heads at the upper and lower boundaries are 0 mH_2O and 2.338 mH_2O, respectively, so that the overall upward hydraulic gradient is equal to 0.0167 that was obtained in other groundwater flow analysis for a specific site. The left-hand boundary, that is, the centerline of the shaft, and the right-hand boundary are impermeable.

We assume that non-sorbing solute continues to be injected at a constant rate. The injection point is within the lining (3.25 m < x < 3.5 m) of the shaft at z=0 meter in the sedimentary rock case. On the other hand, the injection point is within the excavation-disturbed zone (3.5 m < x < 4.5 m) of the shaft at z=0 meter in the granitic rock case. As the boundary conditions for solute transport analysis, no flux of solute is assumed to cross the centerline of the shaft. And, the Neumann boundary condition is given to the other boundaries.

The input values of hydraulic parameters used for the basic case in the numerical analysis for the shaft are shown in Table 1. The hydraulic conductivity of the sound rock mass is assumed to be $1x10^{-8}$ m/sec in both sedimentary rock and granitic rock, while the porosity of the sedimentary rock is 20 times as large as the granitic rock. The hydraulic conductivity of the excavation-disturbed zone is assumed to be 10 times larger than that of the sound rock mass in sedimentary rock, while the hydraulic conductivity of the zone is assumed to be 100 times larger than that of the sound rock mass in granitic rock. The porosity of the excavation-disturbed zone is the same as that of the sound rock mass in both types of rock. The hydraulic conductivity of the backfill material is the same as that of the sound rock. The hydraulic conductivity of the lining is assumed to be $1x10^{-6}$ m/sec in consideration of the deterioration of the concrete. Longitudinal and transverse dispersivities are 10 and 1 meters, respectively, in all the materials. In this study, we did not take the dispersion of the solute into consideration.

Under the above-mentioned numerical conditions, a solute transport analysis was performed. The evaluation point is a horizontal plane at z = 100 meters and the breakthrough curve of the solute flux through the plane in the cases for various specifications of plugs and backfill material was compared to the breakthrough curve in the case where there is no shaft but only the rock mass in the model region.

2.2 Calculated results

Figure 2 shows the calculated breakthrough curves at z = 100 meters for the various numbers of hydraulic plugs in the sedimentary rock concept. In all the cases except those without a shaft and/or plugs, the diameter of the plugs is 13 meters. In the figure, the breakthrough curves are normalized to the flux of solute

TABLE 1. Input Parameters used for Basic Case in the Analysis for Shaft

Material		Hydraulic Conductivity (m/sec)	Porosity (-)
Sedimentary Rock	Sound Rock	1E-8	0.2
	EDZ	1E-7	0.2
Granitic Rock	Sound Rock	1E-8	0.01
	EDZ	1E-6	0.01
Backfill Material		1E-8	0.4
Shore		1E-6	0.2
Plug		1E-11	0.35

injected at z=0 m. The more the number of plugs increases, the slower the solute migrates to the evaluation point. Installing five plugs makes the migration time almost equal to the case without a shaft.

Figure 3 shows the calculated breakthrough curves for the various diameters of plugs in the sedimentary rock concept. In all the cases except those without a shaft, five plugs are installed in the shaft. The figure shows that five plugs with a diameter of more than 13 meters are required.

Figure 4 shows the calculated breakthrough curves for the various hydraulic conductivities of the plugs in the sedimentary rock concept. In all the cases except that without a shaft, five plugs with a diameter of 13 meters are installed in the shaft. The figure shows that a hydraulic conductivity one-order lower than the sound rock is required for the plugs.

Figure 5 shows the calculated breakthrough curves for the different hydraulic conductivities of the backfill material in the sedimentary rock concept. The hydraulic conductivity of the backfill material has almost no influence on the migration time if five plugs with a diameter of 13 meters are installed in the shaft.

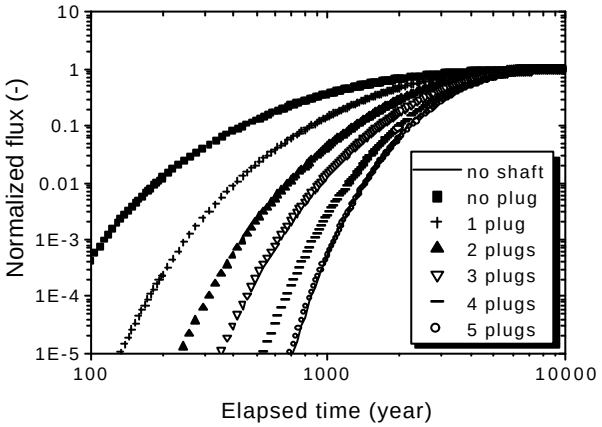

Fig. 2. Calculated breakthrough curves for various numbers of plugs in sedimentary rock concept.

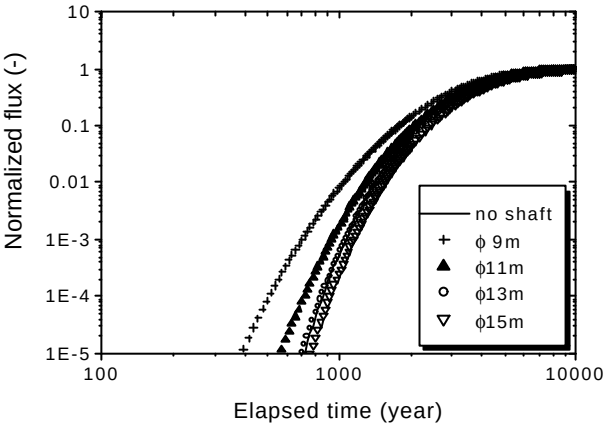

Fig. 3. Calculated breakthrough curves for various diameters of plugs in sedimentary rock concept.

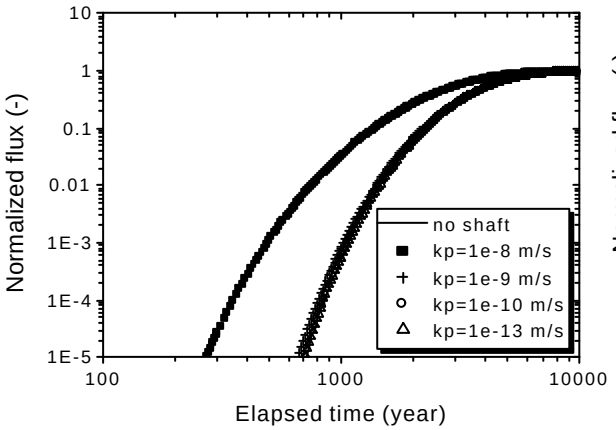

Fig. 4. Calculated breakthrough curves for various hydraulic conductivities of plugs in sedimentary rock concept.

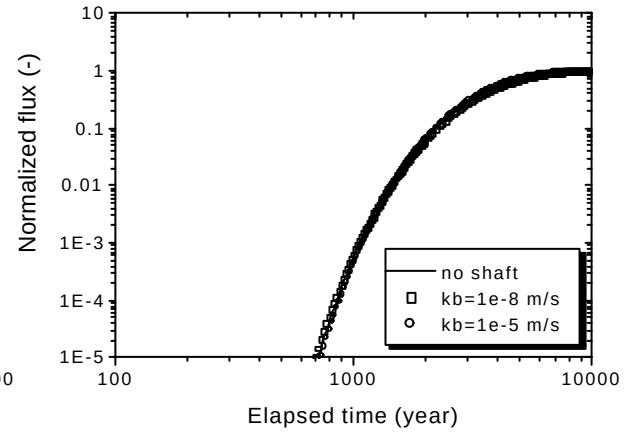

Fig. 5. Calculated breakthrough curves for different hydraulic conductivities of backfill materials in sedimentary rock concept.

Figure 6 shows the calculated breakthrough curves for the various numbers of plugs with a diameter of 13 meters in the granitic rock concept. Unlike the sedimentary rock concept, installing three plugs makes the migration time almost equal to that without a shaft. In that case, the hydraulic conductivity of the plugs is required only to be below that of the sound rock. In the case where the hydraulic conductivity of the backfill material is $1x10^{-8}$ m/sec, the average pore velocity in the backfill material is slow and the solute migrates mainly in the excavation-disturbed zone. On the other hand, in the case where the hydraulic conductivity of the backfill material is $1x10^{-5}$ m/sec, the average pore velocity in the backfill material is relatively high and the solute migrates not only in the excavation-disturbed zone but also in the backfill material. So, if three plugs with a diameter of 13 meters are installed in the shaft, the travel time of the solute to the evaluation point in the case where the hydraulic conductivity of the backfill material is $1x10^{-5}$ m/sec is longer than that in the case where the hydraulic conductivity of the backfill material is $1x10^{-8}$ m/sec.

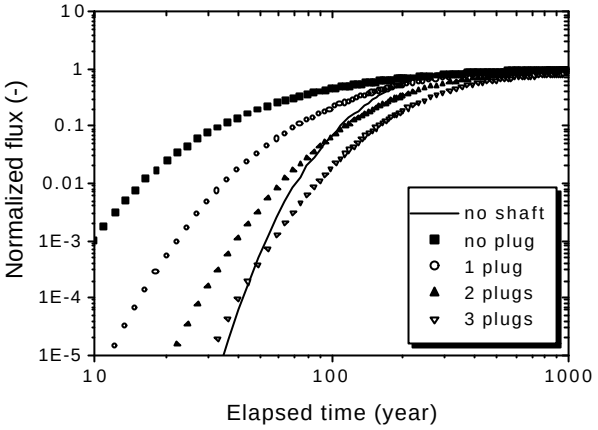

Fig. 6. Calculated breakthrough curves for various numbers of plugs in granitic rock concept.

The requirements for the hydraulic plugs in the shafts obtained in this study are summarized in Table 2. We think that the difference between the calculated results in the sedimentary and granitic rock concepts was caused by the difference between the porosities of both rocks. Namely, the mean pore velocity in granitic rock is 20 times faster than that in sedimentary rock, because the porosity of granitic rock is one twentieth of that of sedimentary rock. If the hydraulic plugs satisfying the requirements shown in the table are installed in the shafts, there is no special hydraulic requirement for the backfill material.

TABLE 2. Hydraulic requirements for plugs in shaft

Specification	Sedimentary rock	Granitic rock
Diameter (m)	13	13
Height (m)	5	5
Number of plugs	5	3
Hydraulic conductivity (m/s)	1E-9	1E-8

3. Hydraulic requirements for backfill material in the emplacement tunnel

3.1 Investigation method

We examined the requirements for the hydraulic conductivity of the backfill material in the emplacement tunnel for the vertical emplacement concept in the sedimentary rock formation. The parametric analysis where the hydraulic conductivity of the backfill material and the direction of the trend flow are selected as parameters is performed on the basis of a groundwater flow simulation with a three-dimensional model.

The model domain is a cube with a side length of 300 meters. An emplacement tunnel and two access tunnels are assumed to be situated in the central part of the domain. Figure 7 shows the expanded vertical section of the numerical model passing the axis of the emplacement tunnel. The diameter and length of the emplacement tunnel are 5.56 meters and about 94 meters, respectively. The diameter and length of the access tunnels are 6 meters and 100 meters, respectively. The emplacement tunnel perpendicularly intersects the access tunnels. There are 17 pits for emplacement under the emplacement tunnel. Figure 8 shows the expanded vertical section of the numerical model perpendicular to the axis of the emplacement tunnel. A buffer material is packed around the waste packages in the pits. A concrete lining of 0.15 meter in thickness is built on the inside of the emplacement tunnel.

The velocity around the pit in the center of the emplacement tunnel was used as an index for evaluation. Five evaluation points were arranged around the pit. Namely, evaluation point A was arranged at the center of the emplacement tunnel and evaluation points B, C, D and E were arranged around the buffer material (*see* Figure 8).

Table 3 shows the numerical conditions used in each simulation case. Case C1 is a basic case. The hydraulic conductivity of the sound rock is $1x10^{-8}$ m/s in all the simulation cases. The excavation-disturbed zones were developed by the excavation of the emplacement tunnel and the access tunnel and not developed by the excavation of the pits following the excavation of the tunnels. The thickness of the excavation-disturbed zones is assumed to be equal to the diameters of the tunnels on the basis of the numerical condition used in our performance assessment of the engineered barrier system. And, the hydraulic conductivity of the excavation-disturbed zones within 0.5 meter of the tunnel wall is assumed to be $1x10^{-6}$ m/s, while the hydraulic conductivity of the other region of the excavation-disturbed zones is $1x10^{-7}$ m/s. Three directions of the trend groundwater flow were selected, namely, the parallel and perpendicular directions to the emplacement tunnel and the direction diagonally upward at 45 deg. to the emplacement tunnel. The hydraulic heads at the surrounding boundaries were prescribed so that the average hydraulic gradient became 0.01 along the direction of the trend groundwater flow.

3.2 Calculated results

The calculated results are also shown in Table 3. When the direction of the trend flow is perpendicular to the emplacement tunnel, the average velocity around the buffer material in case C2 is 0.9 time that in case C1, although the velocity at the center of the emplacement tunnel in case C2 is 26 times that in case C1. When the direction of the trend flow is parallel to the emplacement tunnel, the average velocity around the buffer material in case C4 is 2.4 times that in case C3, although the velocity at the center of the emplacement tunnel in case C4 is 26 times that in case C3. When the direction of the trend flow is diagonal to the emplacement tunnel, the influence of the hydraulic conductivity of the backfill material on the velocities at the evaluation points is almost the same as when the direction of trend flow is parallel to the emplacement tunnel. Anyway, the hydraulic conductivity of the backfill material affects the velocity at the center of the emplacement tunnel significantly but does not affect the velocity around the buffer material very much regardless of the direction of the trend flow.

According to the results of our performance assessment of the engineered barrier system, the leakage of radionuclides from the pits for emplacement is influenced more significantly by the velocity around the pit than by the velocity in the emplacement tunnel. As mentioned above, the hydraulic conductivity of the backfill material of the emplacement tunnel does not greatly affect the groundwater flow around the pits for emplacement. Accordingly, we have concluded that the requirement for the hydraulic conductivity of the backfill material in the emplacement tunnel is not so strict.

4. Conclusions

We could obtain the hydraulic requirements for the backfill and plug materials in the HLW disposal system. However, the requirements are premised on assumed numerical conditions. So, it is very important to collect the data for the hydraulic characteristics of the excavation-disturbed zone, etc. and improve the accuracy of the analysis from now on. Also construction feasibility should be assessed.

Reference

Frieg, B., Marschall, P., Blümling, P., Albert, W., Kull, H. and Liedtke, L., The near-field programme and the tomography and borehole sealing projects, Nagra Bulletin, No.27, pp.18-42, 1996.

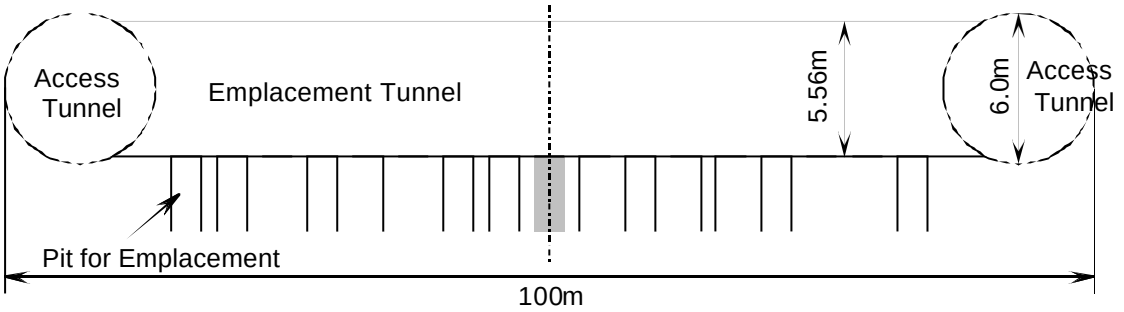

Fig. 7. Expanded Vertical Section passing the Axis of Emplacement Tunnel.

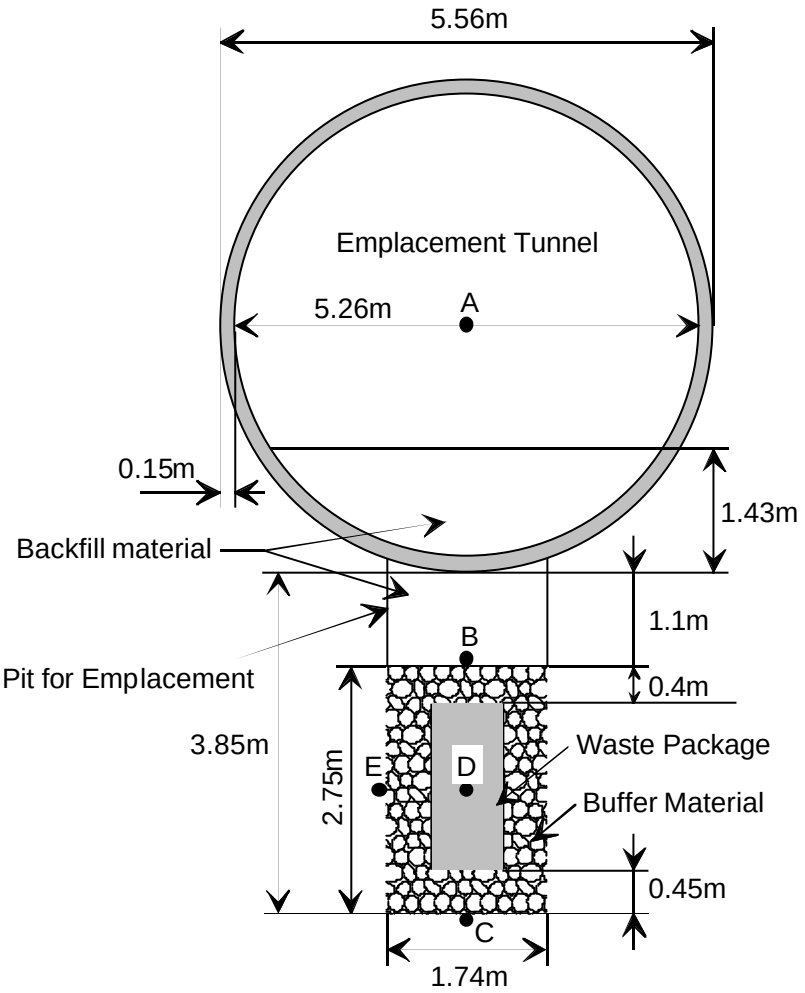

Fig. 8. Expanded Vertical Section perpendicular to the Axis of Emplacement Tunnel.

TABLE 3. Numerical conditions and calculated results in the analysis for hydraulic requirements for backfill material in emplacement tunnel

Case	Numerical condition		Calculated results		
			Velocity at evaluation points (m/sec)		
	Hydraulic conductivity of backfill material (m/sec)	Flow direction	Point A at emplacement tunnel	Point B, C, D and E around buffer material	
				Maximum	Average
C1	1E-8	perpendicular	1.11E-11	2.17E-10	1.10E-10
C2	1E-6	perpendicular	2.85E-10	1.74E-10	9.56E-11
C3	1E-8	parallel	8.04E-11	1.30E-9	6.63E-10
C4	1E-6	parallel	6.84E-9	4.50E-9	1.60E-9
C5	1E-8	diagonal	5.72E-11	9.27E-10	4.88E-10
C6	1E-6	diagonal	4.84E-9	3.35E-9	1.23E-9

J.3：Slides－Clarification of Requirements for Hydraulic Conductives of Backfill and Plug Materials in HLW Disposal Systems

Clarification of Requirements for Hydraulic Conductivities of Backfill and Plug Materials in HLW Disposal Systems

Y. Tanaka (CRIEPI)
R. Masuda (TEPCO)
K. Ando (OBAYASHI)

Background

- In our safety assessment on the geological disposal of HLW, we suppose that the radionuclides leaking from the engineered barrier system migrate through the natural barrier, that is, the rock matrix to the biosphere. Therefore, it is vital to take measures so that the shafts will not become the critical path for migration of radionuclides.
- According to our preliminary design, the total length of the emplacement tunnels will be over 200 kilometers in the vertical emplacement concept. Therefore, the requirement of the material backfilliing the emplacement tunnels will significantly influence the total cost for the construction of a geological disposal facility.

Objectives

- To clarify the number, size and hydraulic conductivity of the plugs and the hydraulic conductivity of the backfill materials required not to make the shafts critical paths
- To clarify the requirements for the hydraulic conductivity of the backfill materials in the emplacement tunnel for the vertical emplacement concept in the sedimentary rock formation

Assumed Premise in Analysis for Shaft

We suppose that the HLW disposal facility is to be built in the center of an impervious geological formation 200 meters thick and hydraulic plugs are installed within 100 meters upward from the bottom of the shafts.

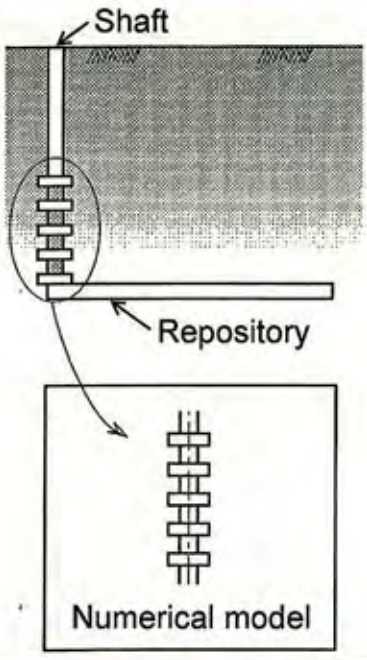

Input Parameters used for Basic Case in the Analysis for Shaft

Material		Hydraulic conductivity (m/sec)	Porosity (-)
Sedimentary rock	Sound rock	1E-8	0.2
	EDZ	1E-7	0.2
Granitic rock	Sound rock	1E-8	0.01
	EDZ	1E-6	0.01
Backfill material		1E-8	0.4
Concrete lining		1E-6	0.2
Plug		1E-11	0.35

Evaluation Criterion

- We calculated the breakthrough curves of the solute flux through the horizontal plane at z = 100 meters for the various specifications of plug and backfill materials.
- The breakthrough curves were compared to the one in the case where there is no shaft but only the rock mass in the model region.

Breakthrough Curves for various Numbers of Plugs in Sedimentary Rock Concept

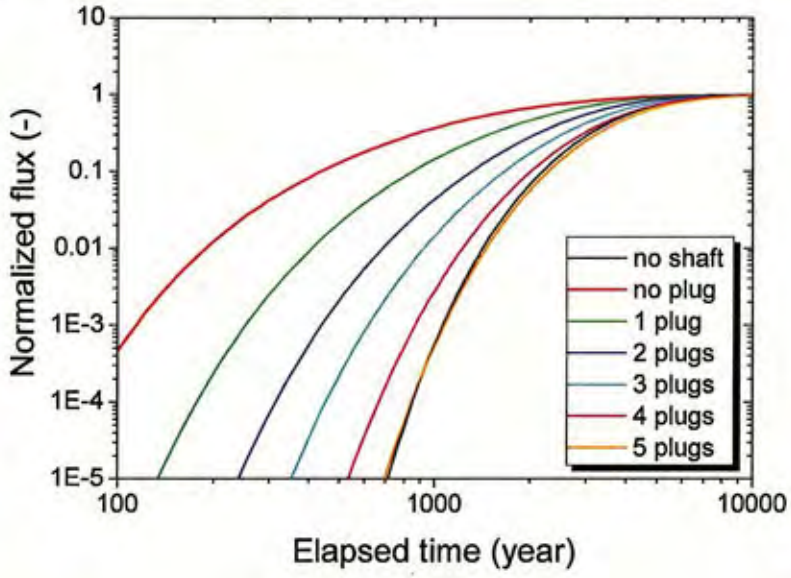

Breakthrough Curves for various Diameters of Plugs in Sedimentary Rock Concept

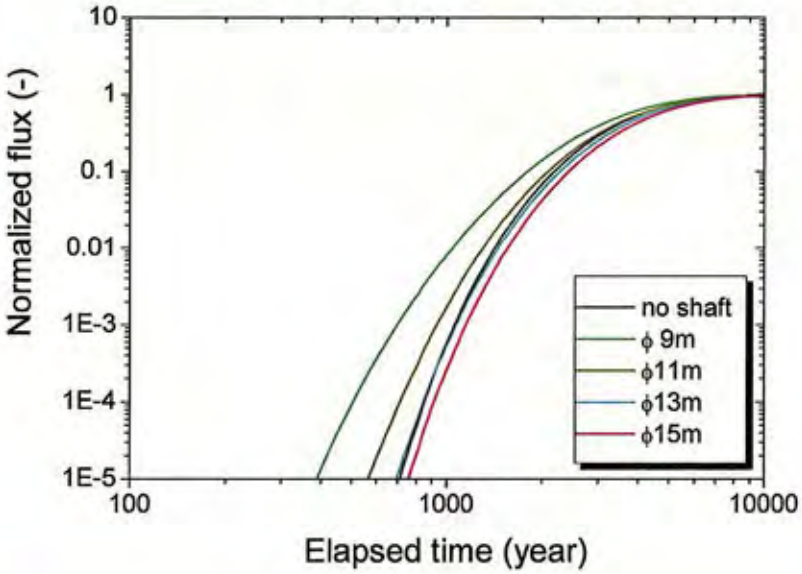

Breakthrough Curves for various Hydraulic Conductivities of Plugs in Sedimentary Rock Concept

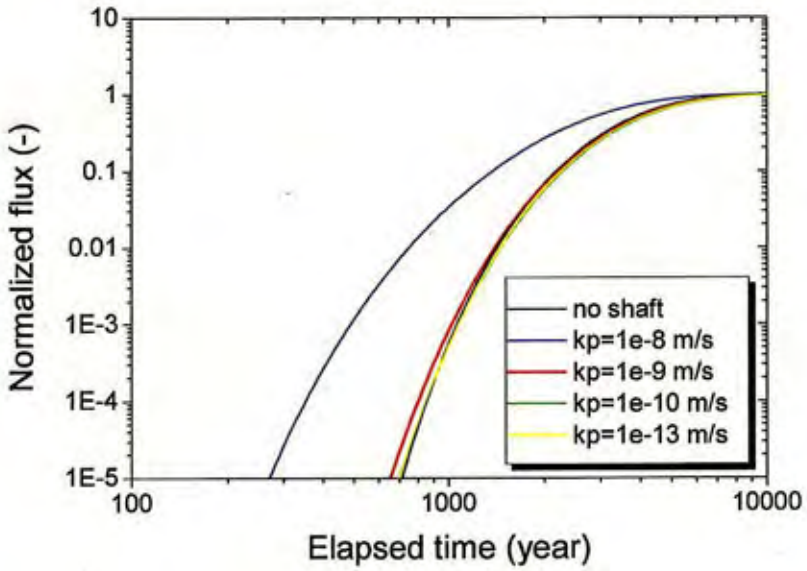

Breakthrough Curves for different Hydraulic Conductivities of Backfill Materials in Sedimentary Rock Concept

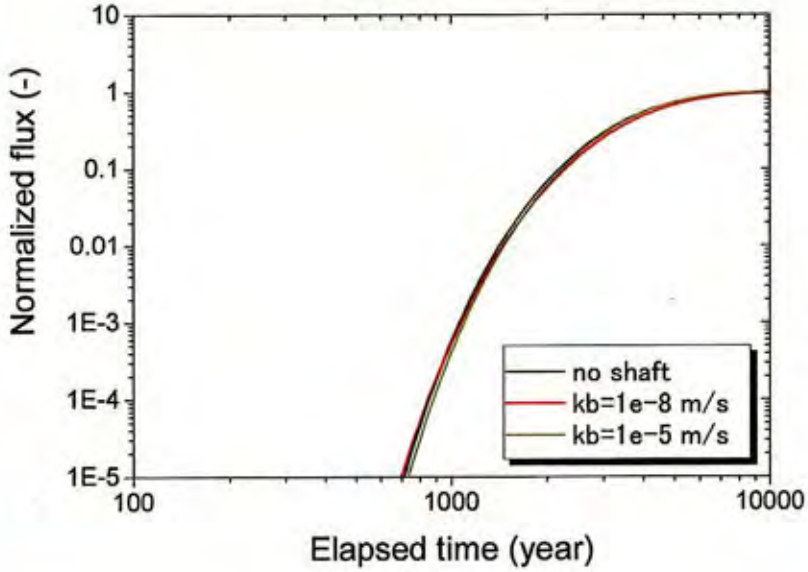

Breakthrough Curves for various Numbers of Plugs in Granitic Rock Concept

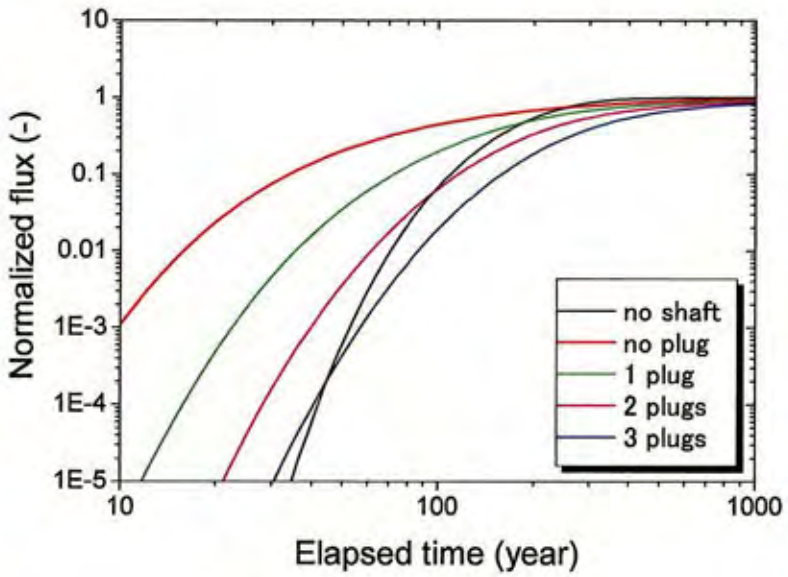

Breakthrough Curves for various Hydraulic Conductivities of Plugs in Granitic Rock Concept

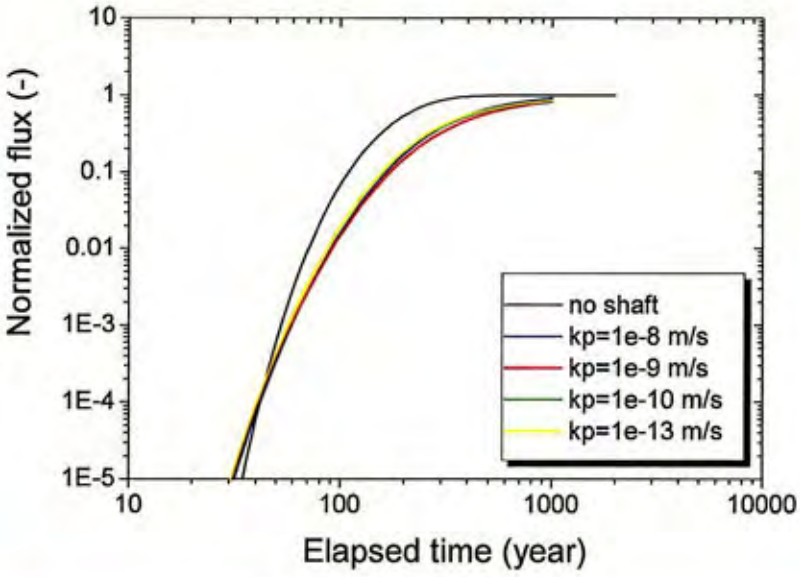

Breakthrough Curves for different Hydraulic Conductivities of Backfill Materials in Granitic Rock Concept

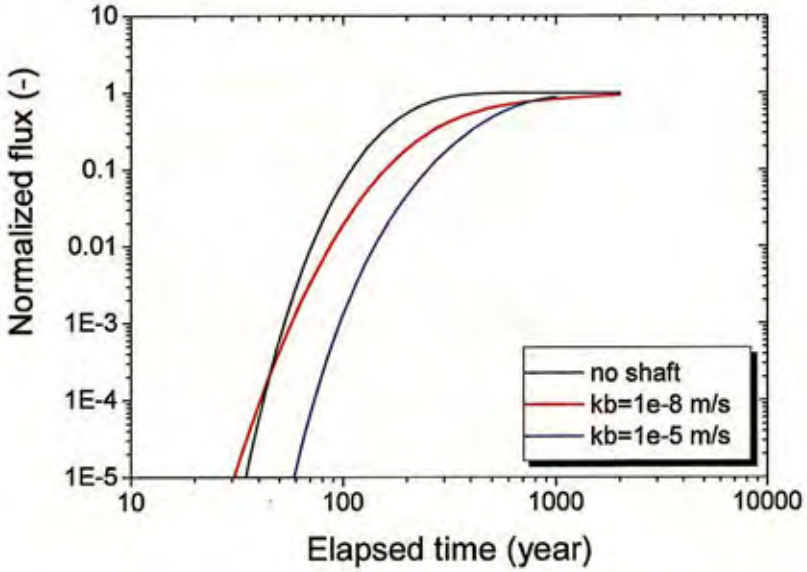

Hydraulic requirements for plugs in shaft

Specification	Sedimentary rock	Granitic rock
Diameter (m)	13	13
Height (m)	5	5
Number of plugs	5	3
Hydraulic conductivity (m/s)	1E-9	1E-8

Analysis for Backfill Materials in Emplacement Tunnel

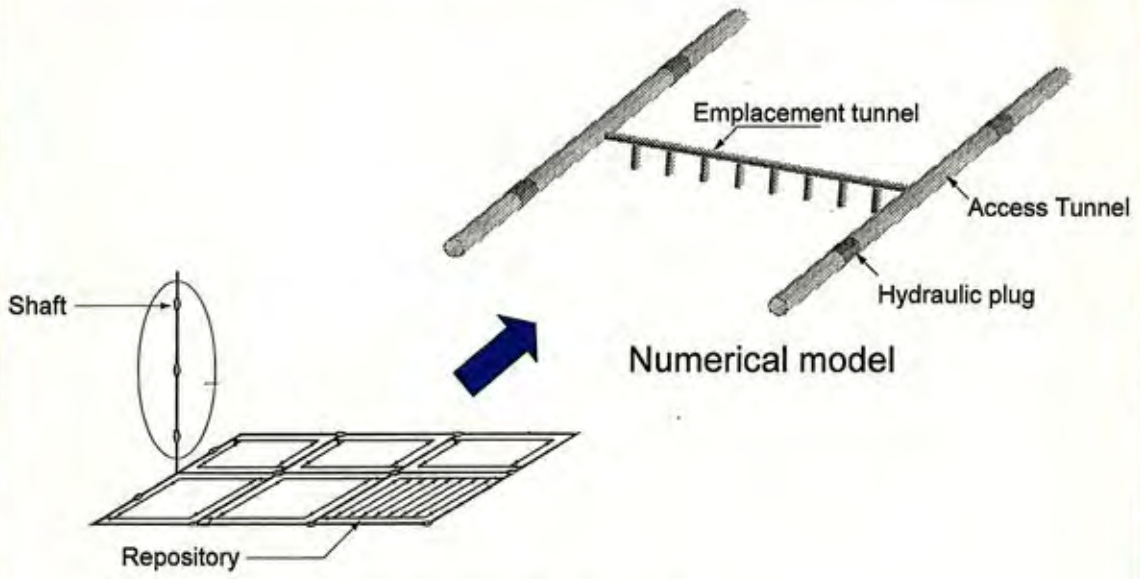

General view of HLW disposal facsility

Numerical Model used in the Analysis for Emplacement Tunnel

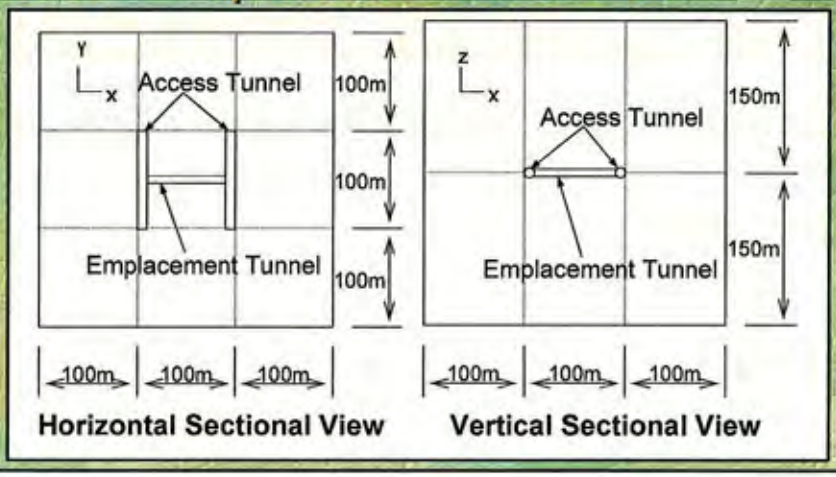

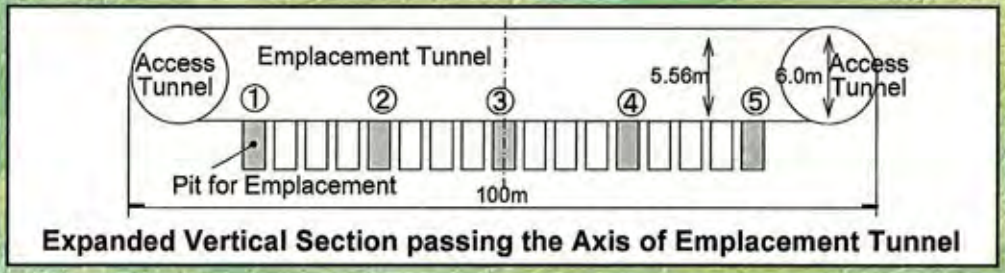

Expanded Vertical Section passing the Axis of Emplacement Tunnel

Finite Element Mesh for the Numerical Analysis

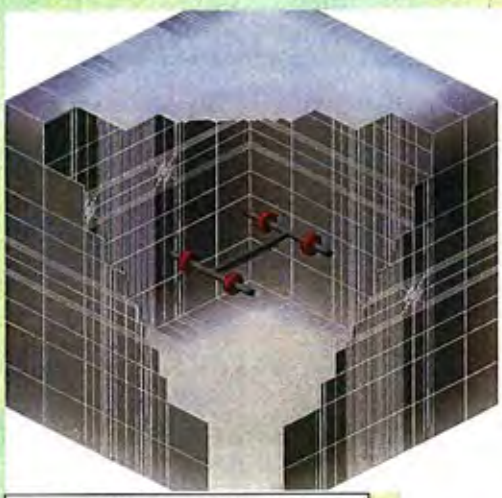

General View of the Model

Expanded View around the Tunnels

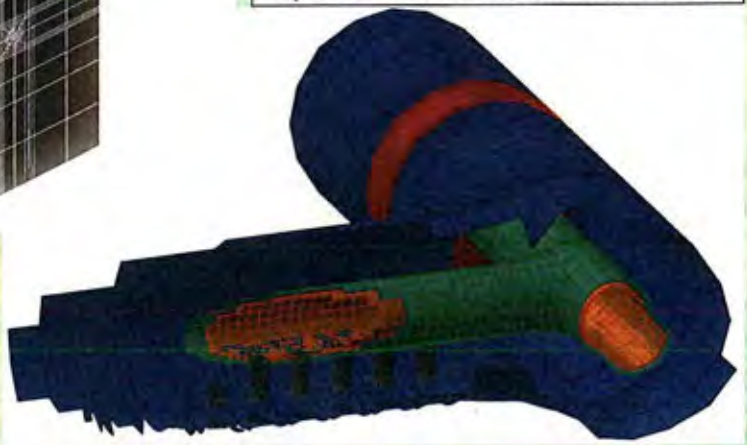

Evaluation Points for Velocity of Groundwater around Emplacement Tunnel

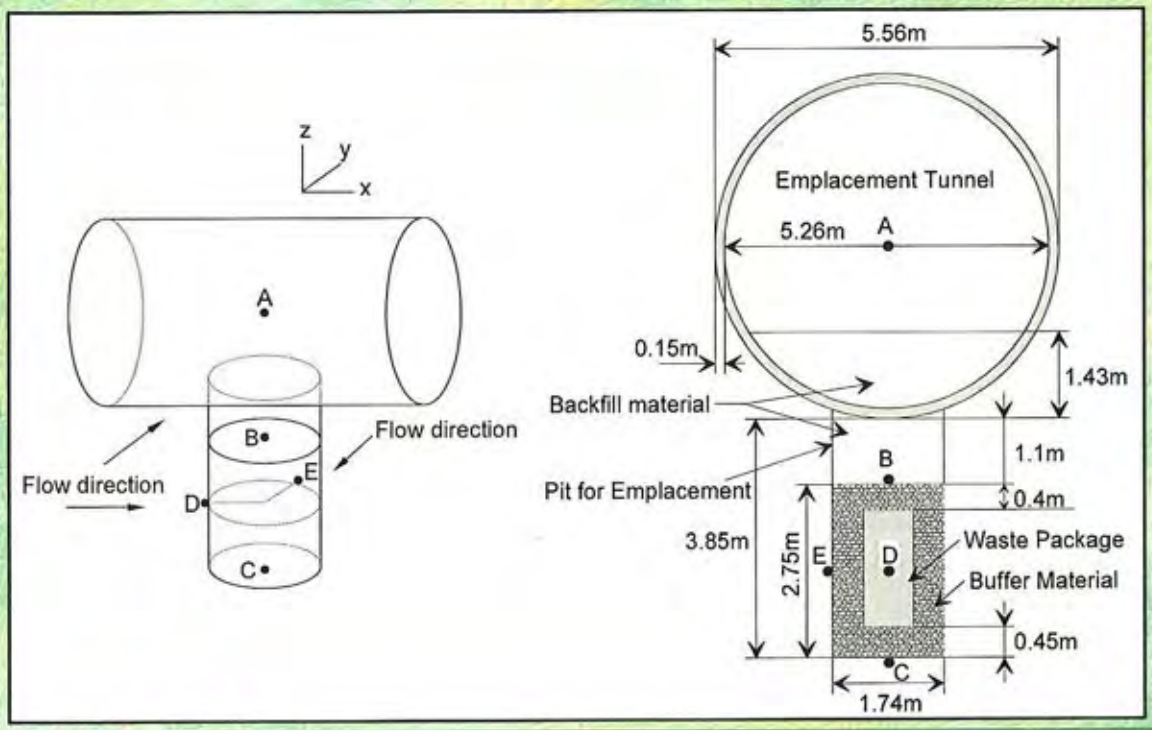

Input Parameters used in the Analysis for Emplacement Tunnel

Material	Hydraulic conductivity (m/sec)
Sound rock	1E-8
EDZ1	1E-6
EDZ2	1E-7
Backfill materials	1E-8 or 1E-6
Buffer materials	1e-10
Concrete lining	1E-6
Plug	1E-13

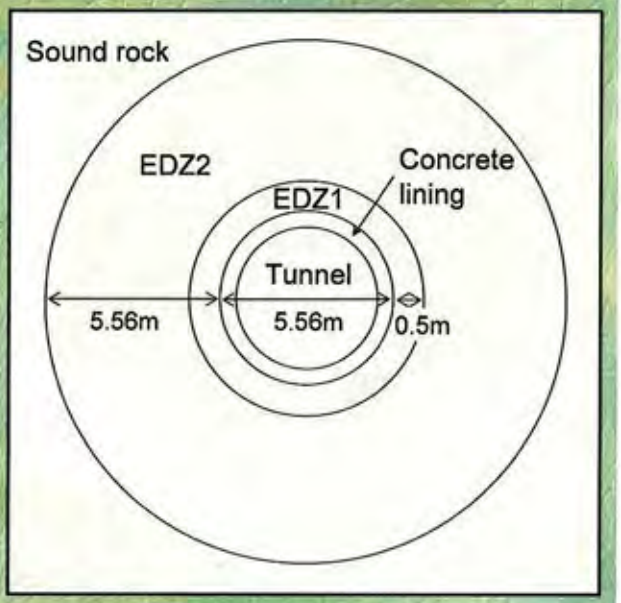

Simulation Cases

Case	Numerical condition	
	Hydraulic conductivity of backfill materials (m/sec)	Flow direction
C1	1E-8	Perpendicular to the emplacement tunnel
C2	1E-6	Perpendicular to the emplacement tunnel
C3	1E-8	Parallel to the emplacement tunnel
C4	1E-6	Parallel to the emplacement tunnel
C5	1E-8	Diagonally upward to the emplacement tunnel
C6	1E-6	Diagonally upward to the emplacement tunnel

Distribution of Velocity around the Emplacement Tunnel (Case C1)

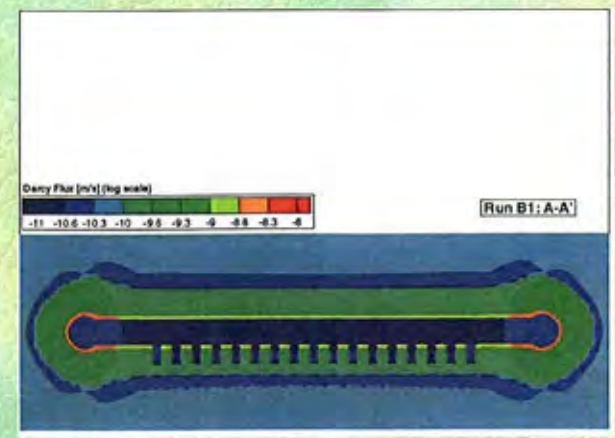

Axial Sectional View

Cross Section View

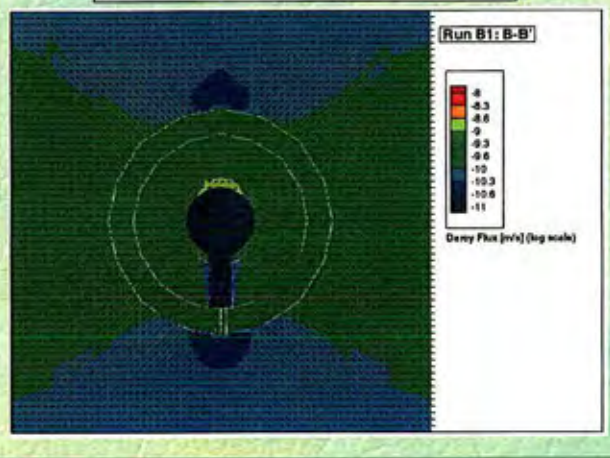

Distribution of Velocity around the Emplacement Tunnel (Case C2)

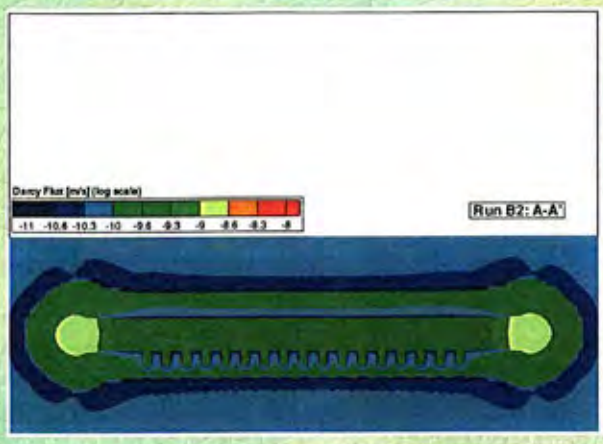

Axial Sectional View

Cross Section View

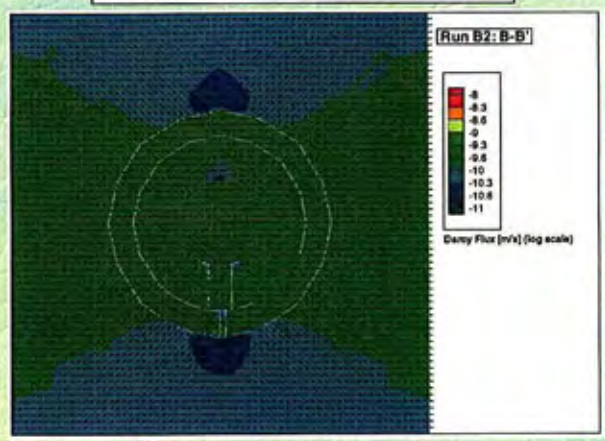

Distribution of Velocity around the Emplacement Tunnel (Case C3)

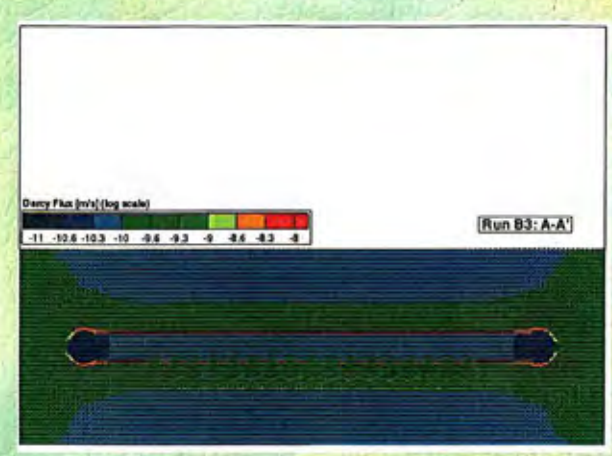

Axial Sectional View

Cross Section View

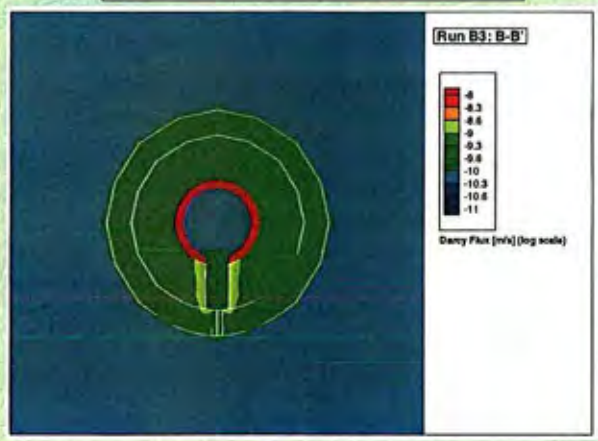

Distribution of Velocity around the Emplacement Tunnel (Case C4)

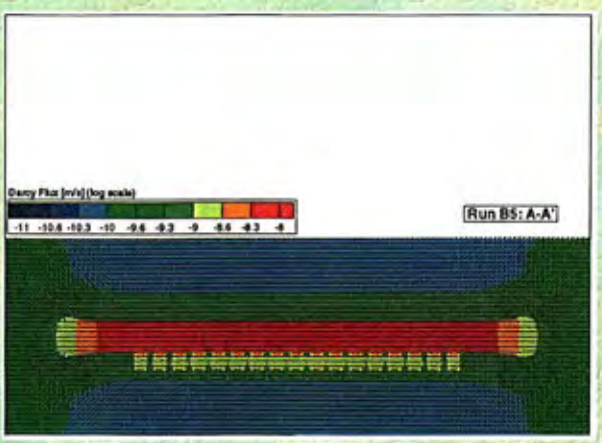

Axial Sectional View

Cross Section View

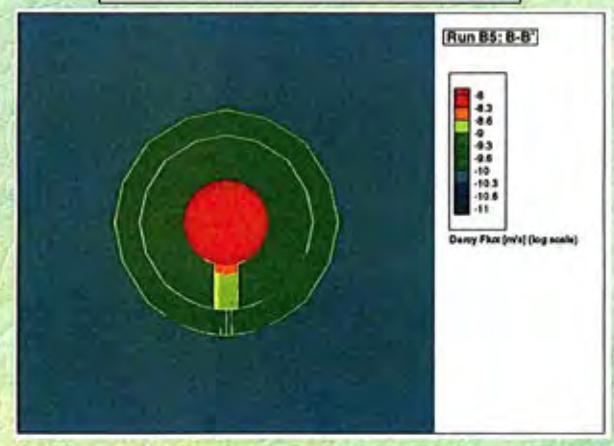

Distribution of Velocity around the Emplacement Tunnel (Case C5)

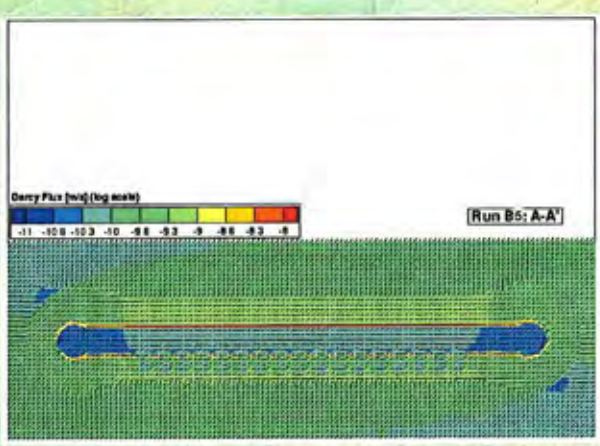

Axial Sectional View

Cross Section View

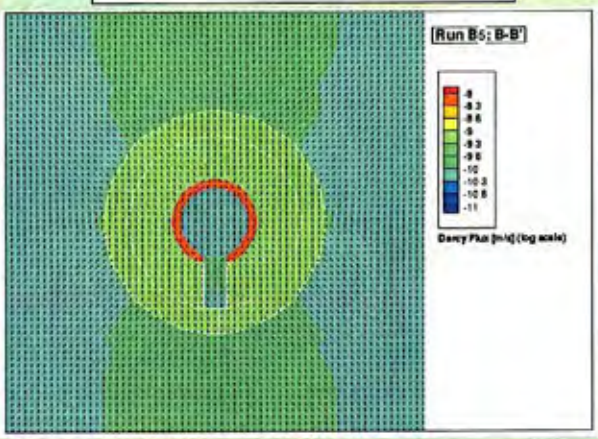

Distribution of Velocity around the Emplacement Tunnel (Case C6)

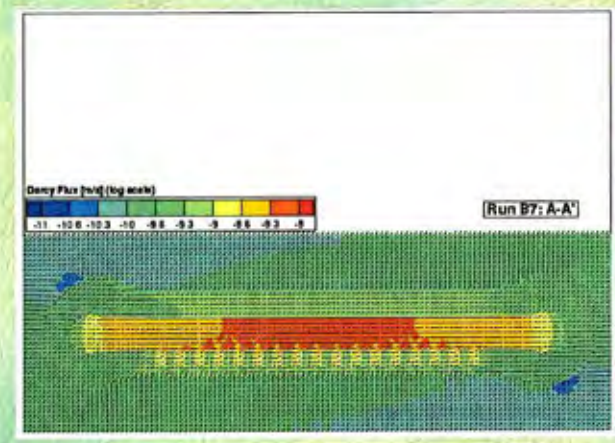

Axial Sectional View

Cross Section View

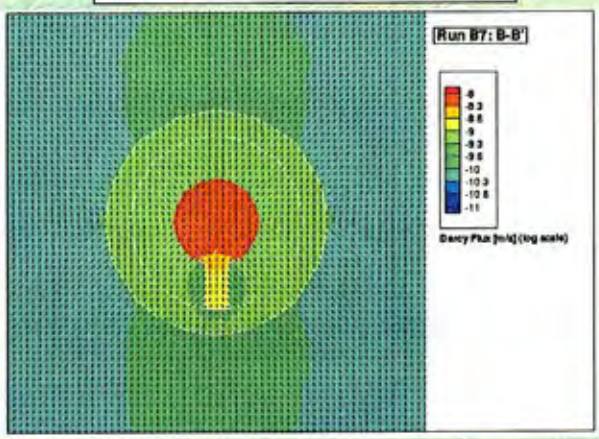

Velocity at the Center of the Emplacement Tunnel

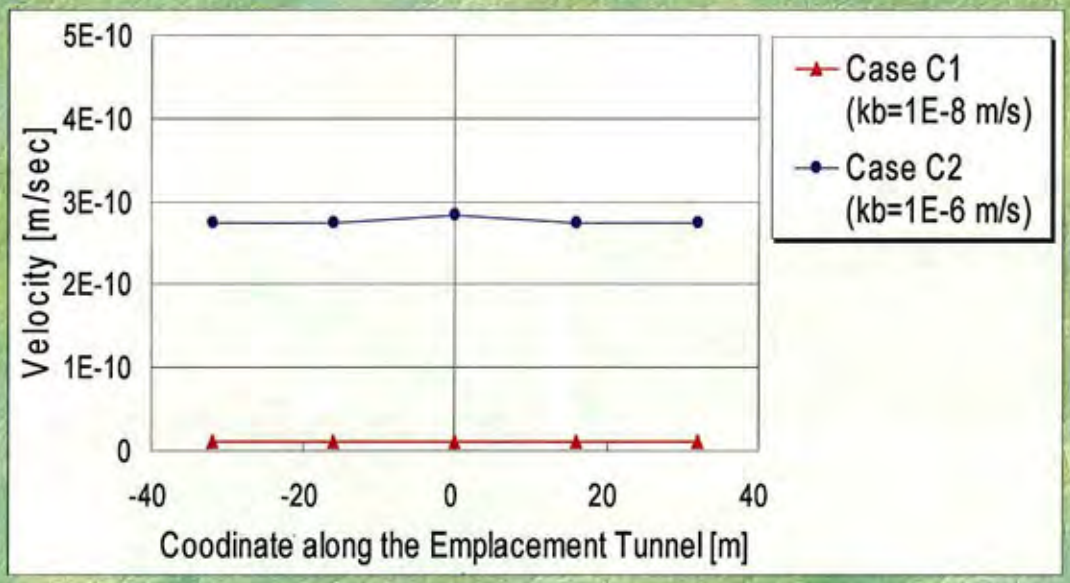

Flow direction : Perpendicular to the emplacement tunnel

Average Velocity at Evaluation Points around Buffer Material

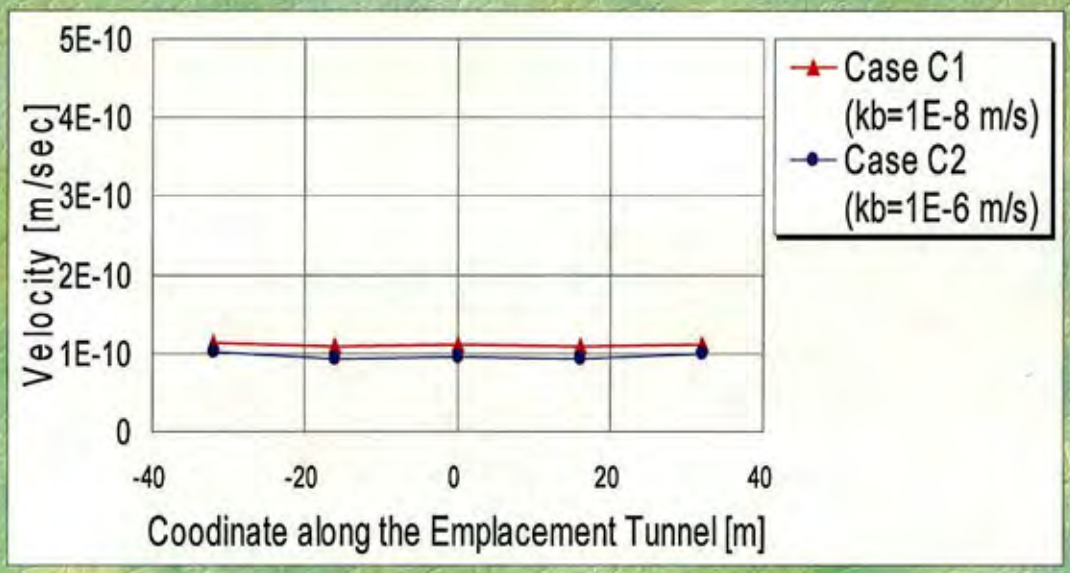

Flow direction : Perpendicular to the emplacement tunnel

Velocity at the Center of the Emplacement Tunnel

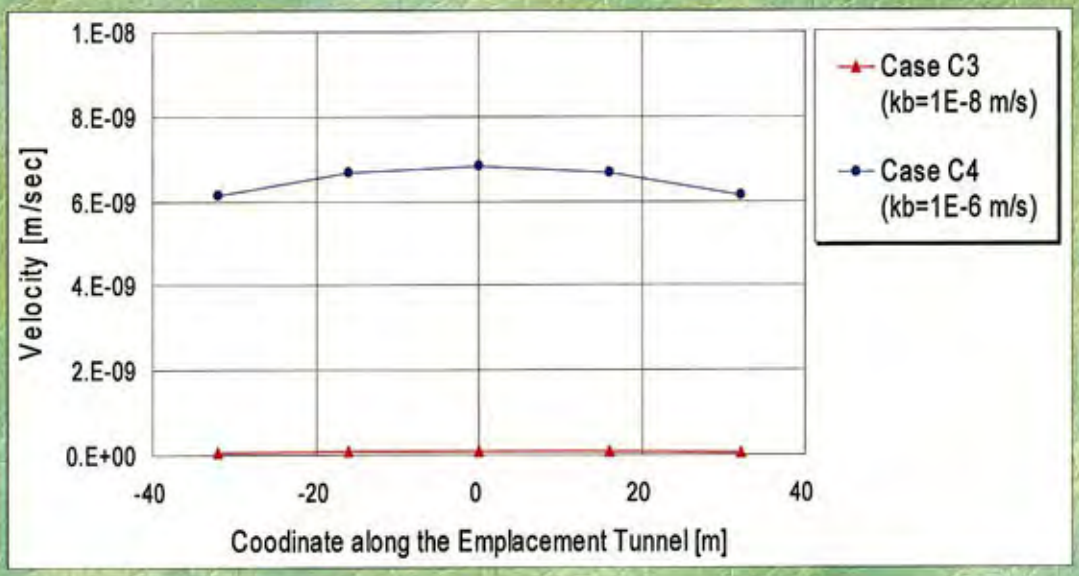

Flow direction : Parallel to the emplacement tunnel

Average Velocity at Evaluation Points around Buffer Material

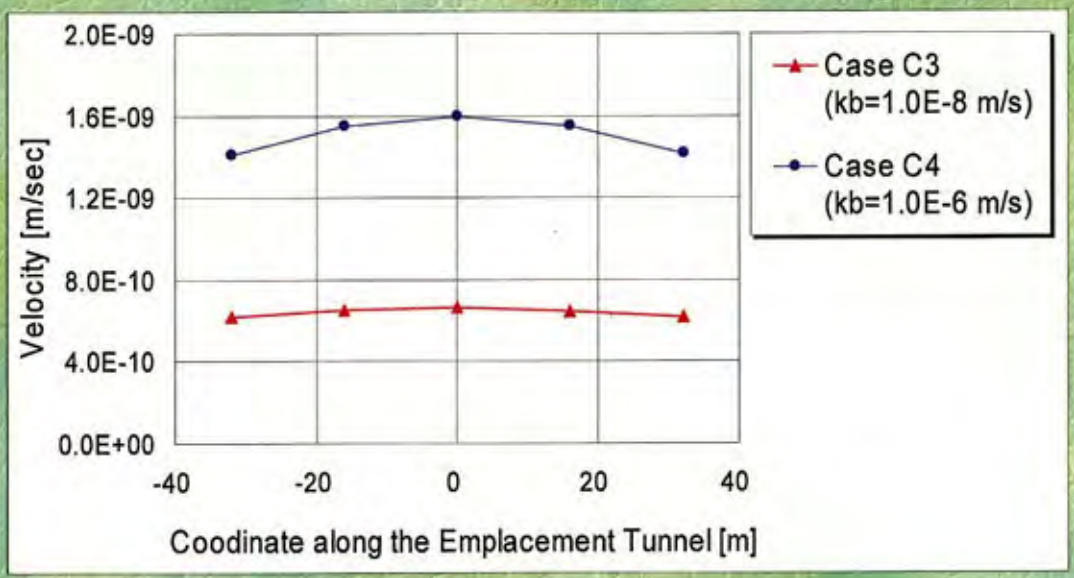

Flow direction : Parallel to the emplacement tunnel

Velocity at the Center of the Emplacement Tunnel

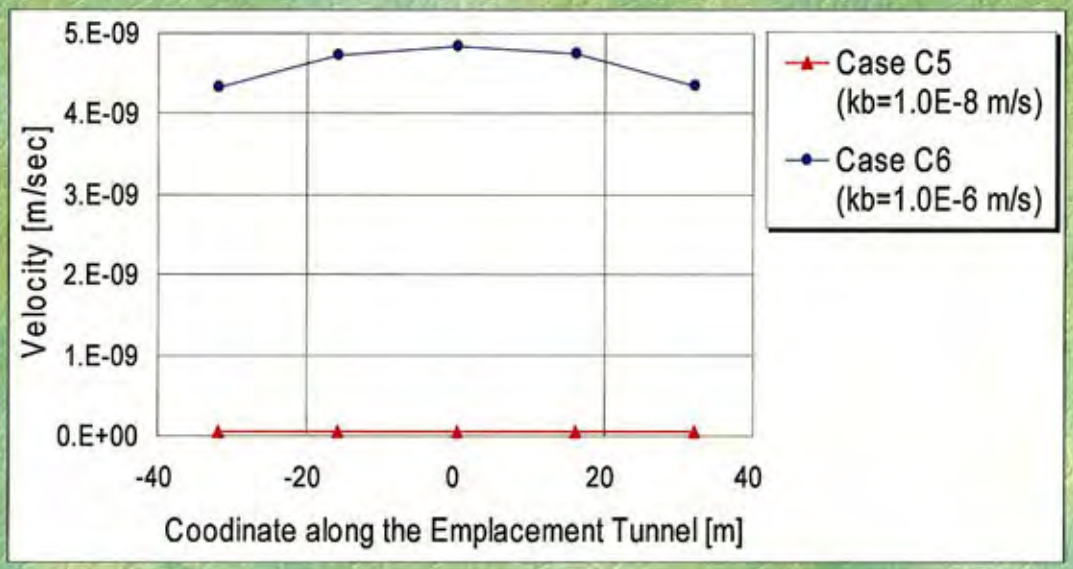

Flow direction : Diagonally upward at 45 deg. to the emplacement tunnel

Average Velocity at Evaluation Points around Buffer Material

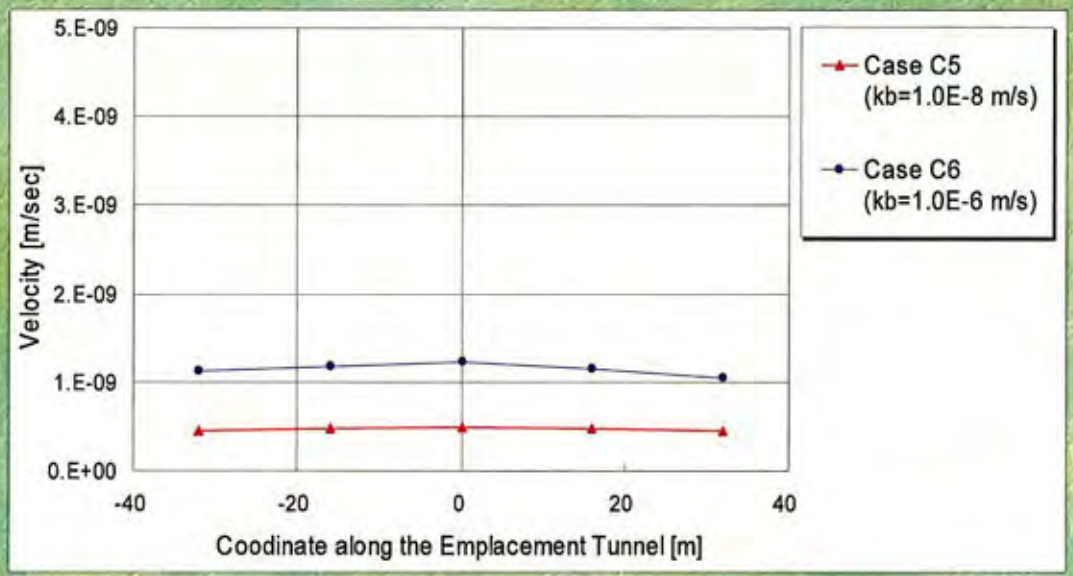

Flow direction : Diagonally upward at 45 deg. to the emplacement tunnel

Numerical conditions and calculated results in the analysis for backfill material in emplacement tunnel

Case	Numerical condition		Calculated results		
			Velocity at evaluation points (m/sec)		
	Hydraulic conductivity of backfill material (m/sec)	Flow direction	Point A at emplacement tunnel	Point B, C, D and E around buffer material	
				Maximum	Average
C1	1E-8	Perpendicular	1.11E-11	2.17E-10	1.10E-10
C2	1E-6	Perpendicular	2.85E-10	1.74E-10	9.56E-11
C3	1E-8	Parallel	8.04E-11	1.30E-09	6.63E-10
C4	1E-6	Parallel	6.84E-09	4.50E-09	1.60E-09
C5	1E-8	Diagonal	5.72E-11	9.27E-10	4.88E-10
C6	1E-6	Diagonal	4.84E-09	3.35E-09	1.23E-09

Radionuclide Release Rate as a function of Velocity around the Buffer Material

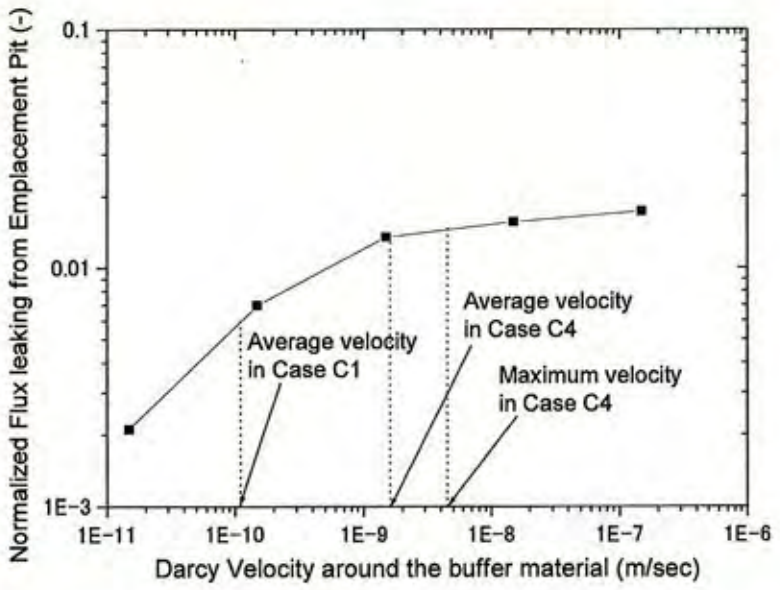

Conclusions

- We could clarify the number, size and hydraulic conductivity of the plugs and the hydraulic conductivity of the backfill materials required not to make the shafts critical paths.
- The requirement for the hydraulic conductivity of the backfill material in the emplacement tunnel is not so strict. .
- The obtained requirements are premised on assumed numerical conditions. So, it is very important to collect the data for the hydraulic characteristics of the excavation-disturbed zone, etc. and improve the accuracy of the analysis from now on. Also construction feasibility should be assessed.